united nations
educational, scientific
and cultural
organization

international atomic
energy agency

the
abdus salam
international centre for theoretical physics

H4.SMR/1330-5

" Sixth Workshop on Non-Linear Dynamics and Earthquake Prediction"

15 - 27 October 2001

Numerical Modeling in Problems of Geophysical Fluid Dynamics.

Part 1.

How Dynamics of the Lithosphere can be Modeled?

A.T. Ismail-Zadeh

International Institute of Earthquake Prediction Theory
and Mathematical Geophysics, Russian Academy of Sciences
Moscow, Russia
e-mail: aismail@mitp.ru

Now at: Institute of Geophysics, University of Karlsruhe
Karlsruhe, Germany
e-mail: Ismail-Zadeh@gpi.uni-karlsruhe.de

Extended Abstract

Geophysical Fluid Dynamics defines a part of Fluid Dynamics which concerns the processes related to the Earth system, namely the processes in atmosphere, oceans, and the solid Earth. During the lecture the term is used in more restrictive sense, defining it as dynamics of very viscous fluid, and hence considering the slow movements in the Earth interiors: in the mantle, asthenosphere, and lithosphere.

The dynamics of the descending lithosphere plays an important part in general dynamics of the lithosphere, because major earthquakes occur in subduction zones. The rheological properties of the lithospheric slab is very complex: it behaves as elastic (or rigid), visco-elasto-plastic and viscous materials at the time scales of seconds to thousand years, of ten thousands to million years, and of more than million years, respectively. The evolution of the descending lithosphere for several million years is considered in the study, and hence the lithospheric slab and its surroundings are approximated by a viscous fluid.

In this lecture we discuss the problems of modeling of the dynamics of the descending lithosphere (see Fig.1).

The first problem in modeling is a simplification of the reality. A model should be as simple as possible, but not oversimplified. A model should present essential features of geological structures under study and reveal major phenomena and processes associated with the structures. All complexities should come later into sophisticated models.

The second problem is to introduce a geometrical shape for the domain under study. We consider two- or three dimensional rectangular domains and various geometries of the lithospheric slab descending in the mantle.

The third problem in modeling is a mathematical statement of the problem under study. We need to employ the equations, which describe very slow movements of the lithosphere and surrounding mantle. The governing equations[†] are presented by the momentum equations (Navier-Stokes equations) of viscous inhomogeneous incompressible flow

$$\rho \left(\frac{\partial \vec{u}}{\partial t} + < \vec{u}, \nabla > \vec{u} \right) = - \nabla p + \mathrm{div} \left(\mu \, e_{ij} \right) + \vec{F}, \tag{1}$$

the incompressibility condition

$$\mathrm{div} \ \vec{u} = 0, \tag{2}$$

the heat balance equation

$$\frac{\partial}{\partial t}(\rho c T) + < \vec{u}, \nabla(\rho c T) > = \mathrm{div} \left(k \ \nabla T \right) + \mu \Phi + \rho Q, \tag{3}$$

the equation of state

$$\rho(t,x) = \rho_*(t,x)(1 - \alpha(T(t,x) - T_0)), \tag{4}$$

and the advection equations for thermally unperturbed density and viscosity

$$\frac{\partial \rho_*}{\partial t} + < \nabla \rho_*, \vec{u} > = 0, \quad \frac{\partial \mu_*}{\partial t} + < \nabla \mu_*, \vec{u} > = 0. \tag{5}$$

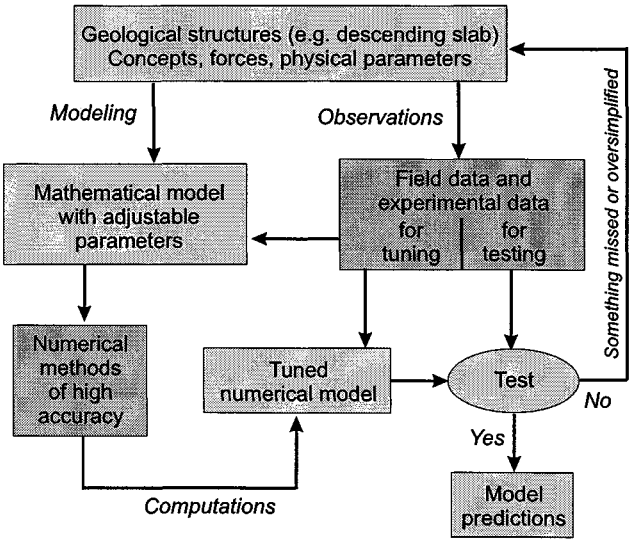

Figure 1: Sketch of Numerical Modeling.

Also we have to adopt a rheological law for the lithosphere. It can be modeled as Newtonian or non-Newtonian fluid. The rheological law may include some other parameters as temperature and/or pressure:

$$\mu(t,x) = \mu_*(t,x)\exp\Big(\frac{E+\rho_* g x_3 V}{RT} - \frac{E_0+\rho_0 g_0 l_0 V_0}{RT_0}\Big). \tag{6}$$

Together with Eqs (1)–(6) we have to consider boundary and initial conditions. At model boundaries we set impenetrability conditions with either perfect slip or no-slip conditions, or prescribe an initial velocity to the part of the model boundaries (in order to investigate effects of horizontal shortening or extension).

The fourth problem is to find solution of the problem stated. The best solution of model problem is known to be an analytical solution. But two-dimensional and even more three-dimensional models do not allow analytical solutions for reasonable physical parameters, and the numerical methods to solve model problems should be employed.

Hence the fifth problem is to find an appropriate numerical methods of high accuracy to solve the system of governing equations together with boundary and initial conditions.

Finite-difference (FDM), finite-element (FEM), spectral and some other methods can be employed to solve such problems. We present and discuss our numerical approach to modeling of lithospheric dynamics. The approach is based on the introduction of a stream function (in 2D case) or a vector velocity potential (in 3D case) and on the application of the Galerkin method (Eulerian FEM) with two- or tri-cubic splines as basis functions for computing the stream function or vector potential. The advection equations are solved by the method of characteristics, and the heat balance equation by a FDM based on a tridiagonal algorithm.

The sixth problem is a comparison of observed data with model predictions. All available

field and experimental data should be splitted into two parts: data for tuning of model parameters and data for testing of the model results. Tuning parameters of the model can be viscosity of the lithospheric slab, its density and temperature structures (which can be recovered from seismotomographic data). The less tuning parameters, the easier to understand effects of the parameters on model results. GPS, stress, heat flow data can be employed as testing parameters of the model.

The attached reprint of the article *"Numerical approach to problems of gravitational instability of geostructures with advected material boundaries"* by Naimark, Ismail-Zadeh and Jacoby describes a numerical technique based on a Galerkin method with tracking of interfaces between layers with distinctive physical properties. The application of the technique to problems of slow movement in the crust and uppermost mantle are considered.

The other attached reprint of the article *"Numerical simulation of three-dimensional viscous flows with gravitational and thermal effects"* by Ismail-Zadeh et al. describes a numerical approach to determine slow viscous flow, introduces a new two-component representation of the vector velocity potential, and discuss algorithms for solving the problem on multi-processor computers.

†The governing equations contain the following variables and parameters: time t; a spatial point x with Cartesian coordinates (x_1, x_2, x_3); velocity vector $\vec{u} = (u_1(t,x), u_2(t,x), u_3(t,x))$; pressure $p = p(t,x)$; absolute temperature $T = T(t,x)$; density $\rho = \rho(t,x)$; viscosity $\mu = \mu(t,x)$; thermally unperturbed density $\rho_* = \rho_*(t,x)$; thermally unperturbed viscosity $\mu_* = \mu_*(t,x)$; acceleration due to gravity g; universal gas constant R; external body force (gravity) per unit volume $\vec{F} = -g\rho\vec{e}_3 = (0, 0, -g\rho)$; unit basis vector $\vec{e}_3$ for the Ox_3 axis; specific heat c; heat conductivity k; coefficient of thermal expansion α; activation energy E; activation volume V; a dissipation function $\Phi = \Phi(t,x)$ representing the rate of heat production due to internal friction; the rate of heat production per unit volume due to nonviscous heat sources $Q = Q(t,x)$; ρ_0, g_0, l_0, E_0 V_0, and T_0 are reference physical parameters.

Geophys. J. Int. (1998) **134**, 473–483

Numerical approach to problems of gravitational instability of geostructures with advected material boundaries

Boris M. Naimark,[1] Ali T. Ismail-Zadeh[1] and Wolfgang R. Jacoby[2]

[1] *International Institute of Earthquake Prediction Theory and Mathematical Geophysics, Russian Academy of Sciences, Warshavskoye sh. 79, kor. 2, Moscow* 113556, *Russia. E-mail: naimark@mitp.rssi.ru*

[2] *Institut für Geowissenschaften, Johannes Gutenberg-Universität Mainz,* D-55099 *Mainz, Germany*

Accepted 1998 March 16. Received 1997 September 5; in original form 1996 August 28

SUMMARY

We present a numerical approach for solving 2-D mantle flow problems where the chemical composition changes abruptly across intermediate boundaries. The method combines a Galerkin-spline technique with a method of integration over regions bounded by advected interfaces to represent discontinuous variations of material parameters. It allows direct approximation of a natural free surface position, instead of *a posteriori* calculation of topography from the normal stress at the upper free-slip boundary. We formulate a model where a viscous incompressible fluid filling a square box is divided into layers (not necessarily horizontal) by advected boundaries, across which the density and viscosity change discontinuously. No-slip or free-slip conditions are assumed at the model sides. The suggested approach, being Eulerian, avoids the difficulties due to material discontinuities at intermediate boundaries, like the Moho or the Earth's surface, and is also free from the deficiencies of the Lagrangian approach, always resulting in mesh distortion. We present two geophysical cases analysed by this technique. The first case concerns the formation of sedimentary basins under the effects of heavy bodies sinking in the asthenosphere and of load due to sedimentary infills. The second case demonstrates the evolution of salt diapirs and shows how their growth is affected by a laterally inhomogeneous sedimentary layer. This numerical approach is well suited for problems of gravitational instability with discontinuities of density and viscosity across advected boundaries.

Key words: advection, diapir, numerical techniques, sedimentary basin.

INTRODUCTION

The problems of gravitational instability involving distinct chemical layers are challenging in geophysical fluid dynamics. Motions of material interfaces separating geomaterials of differing material properties are essential to layered mantle convection, subduction of lithospheric slabs, ascent of mantle plumes, sinking of heavy bodies in the asthenosphere, salt diapirism and many other processes (Jacoby 1970; Römer & Neugebauer 1991; Ribe & Christensen 1994; Schubert, Anderson & Goldman 1995; Naimark & Ismail-Zadeh 1995). The advection of material interfaces was studied analytically for cases of small perturbations and displacements by Biot & Ode (1965), Chandrasekhar (1968), Ramberg (1968), Naimark & Yanovskaya (1976) and Naimark & Ismail-Zadeh (1994). A numerical approach is needed to examine finite displacements of material boundaries. Numerical schemes usually produce errors originating from discontinuities of physical properties, where a step function needs to be advected (Lenardic & Kaula 1993). To minimize such errors, methods of representing these discontinuities were developed by Christensen (1982, 1992) and Naimark & Ismail-Zadeh (1995, 1996).

The problem is simple for the case of discontinuous density, because it enters the right-hand side of the momentum equation. The method of tracer chains suits the purpose, because it reduces the problem of density discontinuities to the integration of relevant terms along the curves (tracer chains).

The problem is much more difficult for the case of discontinuous viscosity. It enters the momentum equation and hence, in the Eulerian approach, must be locally smoothed over several grid steps (e.g. Woidt 1978; Christensen & Yuen 1984; Christensen 1992; Naimark & Ismail-Zadeh 1995, 1996). Additionally, a global filter technique (Lenardic & Kaula 1993) is used to remove overshoots and undershoots of an advected

step function. Dense enough grids are needed to approximate discontinuities by smooth functions, which requires much computer resources.

We present a numerical approach for solving 2-D Stokes' flow problems where physical properties (density and viscosity) change discontinuously across advected boundaries. The approach combines a Galerkin-spline technique with a method of integration over advected layers, where a finite-dimensional space of spline weights is used together with Cartesian coordinate representations of discontinuous viscosity terms. It allows approximation of the natural shape of a free surface, instead of *a posteriori* calculation of its topography from the normal stress at the upper free-slip boundary. We present two geophysical cases analysed by this technique. The first case concerns the formation of sedimentary basins under the effects of heavy bodies sinking in the asthenosphere and of loads due to sedimentary infills. The second case demonstrates the evolution of salt diapirs with laterally homogeneous and inhomogeneous overburdens of sediments.

MODEL CONCEPT

Fig. 1 illustrates the rectangular model region Ω: $0 \le x \le L$, $-H \le z \le 0$, L and H are model width and depth; a Newtonian fluid with variable density ρ and viscosity μ fills this region. Curves $\mathscr{L}_e$, $e = 1, 2, \ldots, E$ divide the model region Ω into several subregions Ω_e, $e = 1, 2, \ldots, E+1$. We assume that each curve $\mathscr{L}_e$ is closed or starts and terminates at the boundary of Ω and has no self-intersections; however, different curves can intersect each other. Fig. 1 shows two curves, $\mathscr{L}_1$ and $\mathscr{L}_2$, and three subregions Ω_1, Ω_2 and Ω_3. In what follows, we consider one curve $\mathscr{L}$ for simplicity, though the number of curves can be arbitrary. We also use dimensionless forms of equations governing the model, so that after the appropriate change of variables the model region Ω occupies the square $0 \le x \le 1$, $0 \le z \le 1$.

Introduce the following notation: $D_x = \partial/\partial x$, $D_z = \partial/\partial z$, $D_{xx} = D_x D_x$, $D_{zz} = D_z D_z$, $D_{xz} = D_x D_z$, $D_t = \partial/\partial t$, and

$$\mathfrak{L}(\mu)\psi = 4D_{xz}\mu D_{xz}\psi + (D_{zz} - D_{xx})\mu(D_{zz} - D_{xx})\psi,$$

$$\mathfrak{L}(\mu; \psi, \varphi) = \mu[4D_{xz}\psi D_{xz}\varphi + (D_{zz}\psi - D_{xx}\psi)(D_{zz}\varphi - D_{xx}\varphi)],$$

$$D(A, \psi) = D_x\psi D_z A - D_z\psi D_x A,$$

where $\psi(x, z, t)$, $\varphi(x, z, t)$ and $A(x, z, t)$ are functions having continuous derivatives entering in the notation.

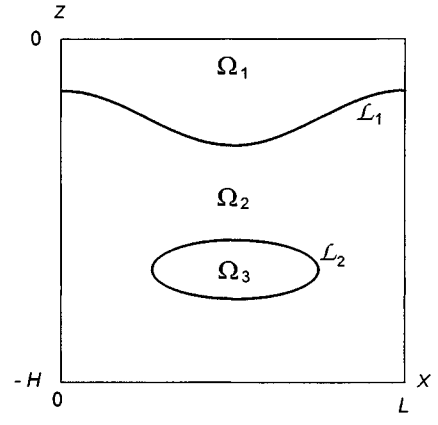

Figure 1. Geometry of the model for the case of two interfaces.

We seek the stream function ψ, density $\rho(x, z, t)$, viscosity $\mu(x, z, t)$ and the family of curves $\mathscr{L}$: $x = x(q, t)$, $z = z(q, t)$ (q is a parameter of points on a curve, $0 \le q \le Q$) satisfying the differential equations (g is the acceleration due to gravity)

$$\mathfrak{L}(\mu)\psi = -gD_x\rho,$$

$$D_t\rho = D(\rho, \psi), \qquad D_t\mu = D(\mu, \psi),$$

$$\frac{dx}{dt} = D_z\psi, \qquad \frac{dz}{dt} = -D_x\psi, \tag{1}$$

the impenetrability and free-slip boundary conditions

$$\psi = D_{xx}\psi = 0 \quad \text{at} \quad x = 0 \text{ and } x = 1,$$

$$\psi = D_{zz}\psi = 0 \quad \text{at} \quad z = 0 \text{ and } z = 1,$$

and initial conditions at $t = t_0$

$$\rho = \rho^0(x, z), \qquad \mu = \mu^0(x, z),$$

$$x(q) = x^0(q), \qquad z(q) = z^0(q).$$

The first equation is the 2-D Stokes equation represented in terms of the stream function ψ, the second and third equations describe the transfer of density and viscosity with the flow, and the remaining equations determine trajectories of points $x(q, t)$ and $z(q, t)$ located at $t_0 = 0$ on the curve $\mathscr{L}_0$.

We define a weak solution of the problem, that is, a solution satisfying an integral relation rather than the equation itself. Let us multiply the first equation in (1) by a function $\varphi(x, z, t)$ satisfying the same boundary conditions as $\psi(x, z, t)$, integrate by parts the left- and right-hand sides of the product twice and once, respectively, and observe that the integral over the model boundary vanishes. Multiply the second and third equations in (1) by functions ϑ and ζ, respectively, and integrate the results. A weak solution of the problem stated above is the set of functions $\psi(x, z, t)$, $\rho(x, z, t)$, $\mu(x, z, t)$, $x(q, t)$ and $z(q, t)$ satisfying the above boundary and initial conditions and the following equations:

$$\iint_\Omega \mathfrak{L}(\mu; \psi, \varphi)\, dxdz = g \iint_\Omega \rho D_x\varphi\, dxdz,$$

$$\iint_\Omega (D_t\rho)\vartheta\, dxdz = \iint_\Omega D(\rho, \psi)\vartheta\, dxdz,$$

$$\iint_\Omega (D_t\mu)\zeta\, dxdz = \iint_\Omega D(\mu, \psi)\zeta\, dxdz,$$

$$\frac{dx}{dt} = D_z\psi, \qquad \frac{dz}{dt} = -D_x\psi, \tag{2}$$

where $\varphi(x, z) \in \mathfrak{B}$, $\vartheta(x, z) \in \mathfrak{R}$ and $\zeta(x, z) \in \mathfrak{R}$ are any functions (called test functions) from sets $\mathfrak{B}$ and $\mathfrak{R}$ properly chosen.

Numerical solutions are obtained in the form of weighted sums of basic bicubic splines. However, bicubic splines, being excellent for the case of smooth unknown functions, become inadequate when these functions are discontinuous. To preserve the accuracy of spline representations for cases of discontinuous unknowns, we suggest the method described below.

Let us represent unknown functions $\rho(x, z, t)$ and $\mu(x, z, t)$ as sums of two functions, one smooth and the other constant over Ω_1 and Ω_2:

$$\rho(x, z, t) = \rho_0(x, z, t) + \rho_1(x, z, t),$$

$$\mu(x, z, t) = \mu_0(x, z, t) + \mu_1(x, z, t),$$

where $\rho_1(x, z, t)$ and $\mu_1(x, z, t)$ have continuous first and second derivatives, whereas $\rho_0(x, z, t)$ and $\mu_0(x, z, t)$ take on constant values in Ω_1 and Ω_2:

$$\rho_0 = \begin{cases} \rho_0^{01}, & \text{if } (x, z) \in \Omega_1, \\ \rho_0^{02}, & \text{if } (x, z) \in \Omega_2, \end{cases}$$
$$\mu_0 = \begin{cases} \mu_0^{01}, & \text{if } (x, z) \in \Omega_1, \\ \mu_0^{02}, & \text{if } (x, z) \in \Omega_2, \end{cases} \tag{3}$$

where ρ_0^{01}, ρ_0^{02}, μ_0^{01} and μ_0^{02} are functions of time, but do not depend on x and z. Let us substitute representations (3) into the first relation in (2) and obtain the result

$$\iint_\Omega \mathfrak{L}(\mu_1; \psi, \varphi)\, dxdz + \mu_0^{01} \iint_{\Omega_1} \mathfrak{L}(1; \psi, \varphi)\, dxdz + \mu_0^{02} \iint_{\Omega_2} \mathfrak{L}(1; \psi, \varphi)\, dxdz = g \iint_\Omega \rho_1 D_x \varphi\, dxdz + g\rho_0^{01} \iint_{\Omega_1} D_x \varphi\, dxdz + g\rho_0^{02} \iint_{\Omega_2} D_x \varphi\, dxdz, \tag{4}$$

and in the interior of any region Ω_i (see Fig. 1)

$$\iint_\Omega (D_t \rho_1)\vartheta\, dxdz = \iint_\Omega D(\rho_1, \psi)\vartheta\, dxdz,$$
$$\iint_\Omega (D_t \mu_1)\zeta\, dxdz = \iint_\Omega D(\mu_1, \psi)\zeta\, dxdz, \tag{5}$$

because $D_t\rho_0 = D_t\mu_0 = D(\rho_0, \psi) = D(\mu_0, \psi) = 0$ in this interior. These equations, together with

$$\frac{dx}{dt} = D_z\psi, \qquad \frac{dz}{dt} = -D_x\psi \tag{6}$$

and with boundary and initial conditions described above, define a weak solution for the case of discontinuous density and viscosity.

NUMERICAL METHOD

Approximations to unknown functions ψ, ρ_1 and μ_1 are represented as linear combinations of basic bicubic splines with unknown coefficients (here and below we assume summation over repeated subscripts taking on the following values: $i, k, m = 1, \ldots, I$; and $j, l, n = 1, \ldots, J$):

$$\psi = \psi_{ij}(t)\, \mathrm{sp}_{ij}(x, z), \qquad \rho_1 = \rho_{ij}(t)\, \widehat{\mathrm{sp}}_{ij}(x, z),$$
$$\mu_1 = \mu_{ij}(t)\, \widehat{\mathrm{sp}}_{ij}(x, z),$$

where $\mathrm{sp}_{ij}(x, z)$ and $\widehat{\mathrm{sp}}_{ij}(x, z)$ are basic bicubic splines satisfying the required boundary conditions. These splines are constructed from basic cubic splines: $\mathrm{sp}_{ij}(x, z) = s_i(x)s_j(z)$ and $\widehat{\mathrm{sp}}_{ij}(x, z) = \hat{s}_i(x)\hat{s}_j(z)$. The basic cubic and bicubic splines used here were described by Naimark & Malevsky (1986). The curve $\mathscr{L}$ is approximated by a polygon whose vertices have coordinates $x_\beta(t)$, $z_\beta(t)$, $\beta = 1, \ldots, B$. These vertices are located on $\mathscr{L}_0$ at $t = t_0$. Let us substitute the above representations into eqs (4) and (5) and integrate forms involving products of basic splines and their derivatives. This results in sets of linear algebraic equations for unknowns ψ_{ij}, ordinary differential equations for ρ_{ij}, μ_{ij}, $x(x^0, z^0, t)$ and $z(x^0, z^0, t)$:

$$\psi_{ij}(t)C_{ijkl} = \rho_{ij}(t)F_{ijkl} + \Psi_{kl}(t),$$
$$\frac{d\rho_{ij}}{dt} G_{ijkl} = \rho_{ij}(t)E_{ijkl}, \qquad \frac{d\mu_{ij}}{dt} G_{ijkl} = \mu_{ij}(t)E_{ijkl},$$
$$\frac{dx}{dt} = \psi_{ij}(t)s_i(x)\frac{ds_j(z)}{dz}, \qquad \frac{dz}{dt} = -\psi_{ij}(t)\frac{ds_i(x)}{dx}s_j(z). \tag{7}$$

Coefficients C_{ijkl} are sums of three terms, $C_{ijkl} = C^1_{ijkl} + C^{01}_{ijkl} + C^{02}_{ijkl}$, where the first term is obtained from μ_1 by substituting its spline representation into the first integral in (4), rearranging sums, and integrating products of splines and their derivatives. The result takes the form

$$C^1_{ijkl} = \mu_{mn}(4A^{110}_{ikm}B^{110}_{jln} + A^{000}_{ikm}B^{220}_{jln} - A^{200}_{ikm}B^{020}_{jln} - A^{020}_{ikm}B^{200}_{jln} + A^{220}_{ikm}B^{000}_{jln}), \tag{8}$$

where

$$A^{pqr}_{ikm} = \int_0^1 s_i(x)^{(p)} s_k(x)^{(q)} \hat{s}_m(x)^{(r)}\, dx,$$
$$B^{pqr}_{jln} = \int_0^1 s_j(z)^{(p)} s_l(z)^{(q)} \hat{s}_n(z)^{(r)}\, dz. \tag{9}$$

Here $(\ldots)^{(p)}$ denotes the derivative of order p of a function $(\ldots)$ and the zero-order derivative is the function itself. The terms C^{01}_{ijkl} and C^{02}_{ijkl} are obtained by integrating products of splines and their derivatives over regions Ω_1 and Ω_2, which results in the forms

$$C^{01}_{ijkl} = \mu_0^{01} \iint_{\Omega_1} \mathfrak{L}(1; s_i(x)s_j(z), s_k(x)s_l(z))\, dxdz,$$
$$C^{02}_{ijkl} = \mu_0^{02} \iint_{\Omega_2} \mathfrak{L}(1; s_i(x)s_j(z), s_k(x)s_l(z))\, dxdz. \tag{10}$$

We see that elements C^1_{ijkl} depend on the continuous term μ_1, but are independent of the curve $\mathscr{L}$. On the other hand, elements C^{01}_{ijkl} and C^{02}_{ijkl} depend on the curve $\mathscr{L}$ and on the constants μ_0^{01} and μ_0^{02}, but are independent of the continuous term μ_1.

Coefficients F_{ijkl} on the right-hand side of the first equation in (7) are obtained by integration:

$$F_{ijkl} = \int_0^1 (\hat{s}_i(x))^{(1)} s_k(x)\, dx \int_0^1 \hat{s}_j(z)s_l(z)\, dz. \tag{11}$$

The term Ψ_{kl} is obtained from the last two integrals on the right-hand side of eq. (4), where φ is set to $s_k(x)s_l(z)$. The sum of these integrals takes the form

$$\Psi_{kl} = g(\rho_0^{02} - \rho_0^{01}) \int_{\mathscr{L}} s_k(x)s_l(z)\, dz \tag{12}$$

explained in detail by Naimark & Ismail-Zadeh (1995).

Coefficients G_{ijkl} and E_{ijkl} entering the second and third equations in (7) are also calculated by integrating basic splines and their derivatives:

$$G_{ijkl} = \int_0^1 \hat{s}_i(x)\hat{s}_k(x)\, dx \int_0^1 \hat{s}_j(z)\hat{s}_l(z)\, dz,$$
$$E_{ijkl} = \psi_{mn}(\mathscr{A}^{001}_{ikm}\mathscr{B}^{100}_{jln} - \mathscr{A}^{100}_{ikm}\mathscr{B}^{001}_{jln}), \tag{13}$$

where $\mathscr{A}^{pqr}_{ikm}$ and $\mathscr{B}^{pqr}_{jln}$ are obtained from A^{pqr}_{ikm} and B^{pqr}_{jln} in eqs (9) with $s_i(x)$, $s_k(x)$, $\hat{s}_m(x)$, $s_j(z)$, $s_l(z)$ and $\hat{s}_n(z)$ replaced by $\hat{s}_i(x)$, $\hat{s}_k(x)$, $s_m(x)$, $\hat{s}_j(z)$, $\hat{s}_l(z)$ and $s_n(z)$, respectively.

The unknowns to be found from eqs (7) are the following: $\rho_{ij}(t_s)$, $\mu_{ij}(t_s)$, $\psi_{ij}(t_s)$, $x_\beta(t_s)$ and $z_\beta(t_s)$, $s = 1, 2, \ldots, S$. The second, third, fourth and fifth relationships in (7) constitute the set of ordinary differential equations (ODE) for unknowns ρ_{ij}, μ_{ij}, x_β and z_β. We solve this set by the fourth-order Runge–Kutta method. The right-hand sides of these equations include unknowns ψ_{ij} found from the first set of equations in (7). Initial values $\rho_{ij}(t_0)$ and $\mu_{ij}(t_0)$ are derived from the conditions

$$\rho_1(x, z, 0) = \rho_{ij}(0)\hat{s}_i(x)\hat{s}_j(z), \qquad \mu_1(x, z, 0) = \mu_{ij}(0)\hat{s}_i(x)\hat{s}_j(z)$$

by using spline interpolation programs. Let us describe the calculation of the right-hand sides. Assume that the unknowns have been calculated at $t = t_s$. Use eqs (8)–(10) to find the matrix C_{ijkl} and eqs (11) and (12) to compute the right-hand sides of the first set in (7). Solve this set for ψ_{ij} and use the values so found, together with eqs (13), to calculate the right-hand sides of the above ODE.

Coefficients (9), (11) and (13) can be computed once and used in all calculations. Certain difficulties arise in eqs (10). The integrals in eqs (10) depend on the curve $\mathscr{L}$, changing with time. We reduce calculations of the forms (10) to direct integration of polynomials over regions bounded by the curve $\mathscr{L}$ and model boundaries; these polynomials are products of splines and their derivatives. To clarify this reduction, consider Fig. 2. This figure shows part of a rectangular grid, the curve $\mathscr{L}$ passing through it, and parts of Ω_1 and Ω_2. The integrals in eqs (10) can be treated as sums of integrals over all grid squares. They are easily computed for squares that are not intersected by $\mathscr{L}$. When a grid square is intersected by the curve, as shown in the figure, the integration is carried out over a region bounded by the square sides and the part of $\mathscr{L}$ in this square. This is done by summing up integrals over all trapezoids bounded by the edges of the polygonal curve $\mathscr{L}$, vertical lines and horizontal segments of the lower grid square side; one such trapezoid is shaded in Fig. 2. The integral over each trapezoid is computed directly by repeated integration of polynomials. Obviously, horizontal trapezoids are treated instead of vertical ones when $\mathscr{L}$ passes through a square from top to bottom. The crucial part of this procedure is the analytical integration over regions whose boundary includes $\mathscr{L}$, which can intersect grid squares in many ways.

Let us discuss the conditions at advected material boundaries. Physically, velocity and stress are continuous across these boundaries. It follows that the viscosity discontinuities across the same boundaries lead to discontinuity of the second invariant of strain rate. In the approach described here the second derivatives of the stream function ψ are continuous, which can look inconsistent with the physical conditions. However, the suggested algorithm leads to fitting these conditions with a continuous ψ, which results in a ψ smoothed over a chosen grid. Overshoots and undershoots of a stream function so found are not as great as might be expected, because the algorithm fits these conditions for second partial derivatives of ψ, rather than for ψ itself.

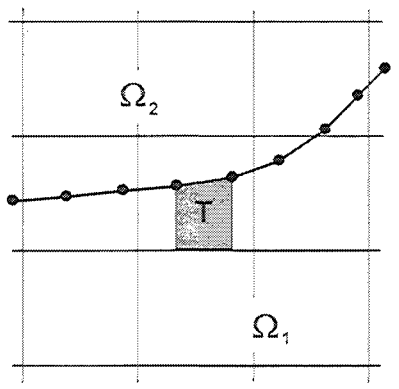

Figure 2. A sketch of the curve passing through a rectangular grid. A current trapezoid T is shaded. The integrals in eqs (10) are calculated as sums of integrals over all trapezoids in the grid square intersected by the curve.

It is, of course, impossible to formulate strictly conditions at free boundaries in the stream function approach, because the order of equations changes when viscosity equals zero. However, when viscosity at one side of a surface is sufficiently low compared to that at the other side, the algorithm still works and leads to correct results. This is verified here in the case of isostatic adjustment in a layered medium. We call boundaries of this kind 'free', to emphasize that they are approximations to physical free boundaries.

Let us note that an interface $\mathscr{L}$, being advected, stretches or compresses, so that the distance between adjacent vertices of its polygonal representation can become too long, and computations lead to erroneous results or deteriorate. To avoid this, we periodically update the polygonal line $\mathscr{L}$. Denote by $|\mathscr{L}|$ the length of $\mathscr{L}$ and by n the number of its vertices. New vertices are placed on $\mathscr{L}$ with the step $h = |\mathscr{L}|/(n-1)$ along it. This results in an almost uniform spacing of vertices on $\mathscr{L}$ at any time step.

VERIFICATION OF THE METHOD

An exact solution of eqs (4)–(6) is unknown even for the simplest cases and boundary conditions. Previous methods were tested for eqs (4) and (5) separately (Ismail-Zadeh, Naimark & Lobkovsky 1996; Naimark & Ismail-Zadeh 1996). The suggested algorithm and codes were verified by comparing numerical results with experimental data and analytical results from the linear theory of the Rayleigh–Taylor instability.

We studied a model of viscous layers with stable density stratification and used data employed in the experimental isostatic test performed by Ramberg (1968). In Ramberg's physical experiment a heavy syrup was supporting a less dense layer of a silicone putty. Initially, a sinusoidal deflection was prescribed at the free surface, whereas the interface between the substratum of syrup and silicone putty was straight and horizontal. The experiment showed that the free surface tended to flatten, and the interface was deflected into a wave. After passing a maximum amplitude, the secondary wave at the interface began to flatten until a stable equilibrium was attained.

We modelled this experiment as follows. The model region was divided into three layers by two curves: $\mathscr{L}_1$: $0 \le x \le L$, $z = 0.105 + 0.077\cos(2\pi x/L)$, and $\mathscr{L}_2$: $0 \le x \le L$, $z = 0.07$. The densities, viscosities and thicknesses of the layers are shown in Table 1. Curve $\mathscr{L}_1$ approximates a free surface; the wavelength of the perturbation λ equals model width L. We used two rectangular grids (20×25 and 46×48) and obtained the same results. The pattern of layers obtained numerically is very close to the experimental results of Ramburg (1968).

Fig. 3 shows an amplitude of wave versus time at the upper boundary and the interface obtained from measurements and

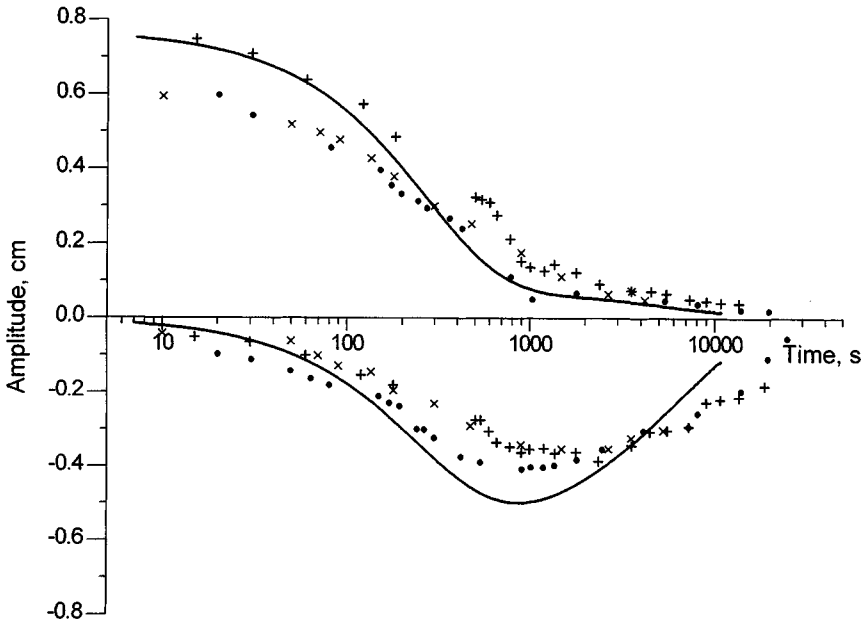

Figure 3. Amplitude versus time for a model of isostatic adjustment in a layered medium. Solid lines show results obtained by the suggested numerical model. Points and crosses represent results from three experimental runs (Ramberg 1968, Fig. 25).

Table 1. Nomenclature of and values used in the model.

Notation	Meaning	Value
λ	wavelength of the perturbation, m	0.136
η	amplitude of the perturbation, m	0.0077
h_1	thickness of the upper layer, m	0.031
h_2	thickness of the middle layer, m	0.035
h_3	thickness of the lower layer, m	0.07
ρ_1	density of the upper layer, kg m^{-3}	0
ρ_2	density of the middle layer, kg m^{-3}	1.25×10^3
ρ_3	density of the lower layer, kg m^{-3}	1.44×10^3
μ_1	viscosity of the upper layer, Pa s	10^2
μ_2	viscosity of the middle layer, Pa s	8.4×10^4
μ_3	viscosity of the lower layer, Pa s	4.2×10^3

the numerical test. The solid lines calculated by the suggested method are indistinguishable from theoretical curves predicted by the linear theory of gravitational instability (Ramberg 1968; Naimark & Yanovskaya 1976). We also see that the computed curves agree closely with experimental data.

EFFICIENCY OF THE METHOD

We analysed two numerical approaches, one proposed previously by Naimark & Ismail-Zadeh (1995), hereinafter called 'old', and that suggested in this paper, called 'new', for the case of a model consisting of three layers. This model is sketched in Fig. 4(a) with the grid used in the calculations. Region 1 has zero density and low viscosity; region 2 is highly viscous, heavy and thin. We call this region thin because it contains two or three grid levels in the z direction. Region 3 is less dense and viscous than region 2. The values of the dimensionless model parameters are presented in Fig. 4(a). Figs 4(b) and (c) show the positions of layer boundaries calculated by the 'old' and 'new' methods at different times.

We see that the 'old' method leads to erroneous perturbations of advected boundaries. It is seen that these perturbations grow with time, while they are absent when the positions of the boundaries are calculated by the 'new' method. Subsequent calculations by the 'old' method lead to an almost instant deterioration of the pattern when time reaches a threshold (in this case about 3000), whereas the layered pattern remains adequate with the 'new' method.

The deficiency of the 'old' method in cases of thin layers can be explained as follows. When the number of grid points across a layer is small, overshoots and undershoots of viscosity lead to large errors in computing the stream function, hence to erroneous velocities controlling advection of boundaries. The values of viscosity at some points can even become negative (as in this test where the viscosity changes from 1 to 1000 across the upper boundary). Naturally, negative viscosity results in erroneous velocities. This effect leads to the deterioration of the overall pattern. On the other hand, there are no overshoots and undershoots of viscosity in the 'new' method. Viscosity remains constant in each of the advected regions.

It is possible to obtain correct results by the 'old' method with denser grids, advanced approaches to smoothing viscosity across the boundaries, and very small time steps. However, the computer resources required will become much greater than those needed in the 'new' method.

SAMPLE CALCULATIONS

Sinking of heavy bodies and sedimentary basin formation

In the magmatism–eclogitization mechanism of sedimentary basin evolution (Lobkovsky *et al.* 1993; Ismail-Zadeh *et al.* 1996) eclogitic bodies evolve from magmatic melts accumulated

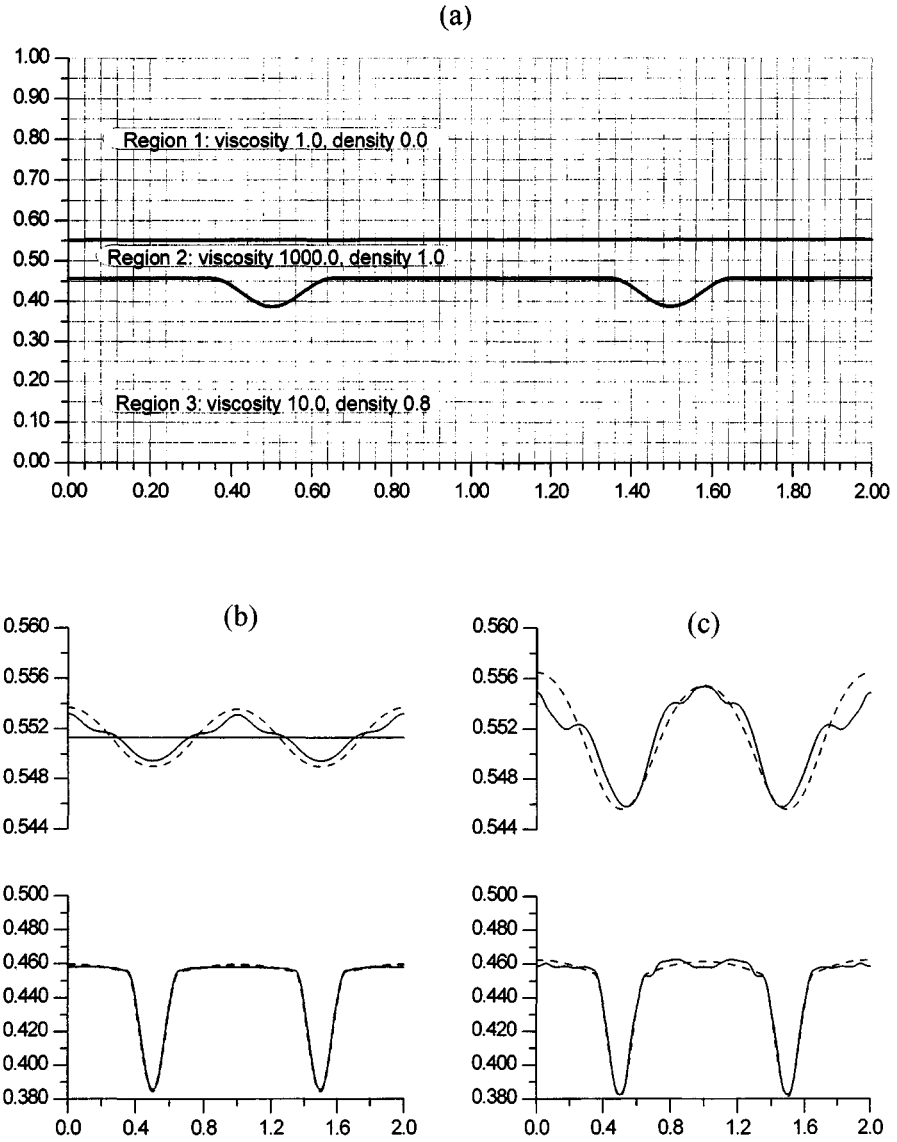

Figure 4. Testing the 'old' and 'new' numerical approaches for the case of a layered model with a heavy, highly viscous layer and a 'free' surface. (a) A sketch of the model and the grid chosen for calculations. The curves depict initial positions of boundaries between layers. (b) The positions of upper and lower boundaries, shown separately and appropriately scaled, at times 479.5 ('old', solid lines) and 473.7 ('new', dashed lines). (c) The same for times 2525.0 ('old') and 2421.0 ('new').

at a depth of 60–80 km in a post-rift phase. These bodies, being denser than the surrounding material, sink in the asthenosphere and induce viscous flows that change surface topography and lead to the formation of sedimentary basins. At least three boundaries where physical properties are discontinuous should be introduced in this model: $\mathscr{L}_1$, the 'free' surface; $\mathscr{L}_2$, the sediment/basement interface; and $\mathscr{L}_3$, the heavy body/asthenosphere interface. Naimark & Ismail-Zadeh (1995) described a similar model where sediments were absent and where the surface topography was calculated *a posteriori* from the normal stress at the upper free-slip surface. The present model includes sedimentary infill and viscosity discontinuities.

The model of sedimentation, chosen here for its simplicity, is based on two assumptions: (1) the depression is filled by sediments instantaneously; (2) this filling stops when the upper level of sediments achieves the value prescribed by a constant *a*. Sediments in this model appear 'from nowhere'; we do not consider processes leading to sedimentation. However, the law of conservation of mass is not violated: the initial mass remains constant, and the new mass is added by sedimentation processes. Note that it is quite easy to incorporate other models by introducing the rate of sedimentation or considering mechanisms based on the shape of the free surface.

According to this model, boundaries $\mathscr{L}_1$ and $\mathscr{L}_2$ are initially (at $t = 0$) coincident with straight horizontal lines $z = b$, where $b < 1$ is a constant. Boundary $\mathscr{L}_1$ is deflected by the viscous flow, and boundary $\mathscr{L}_2$ is calculated in the following manner. Denote by $z_1 = f_1(x, t)$ the function representing curve $\mathscr{L}_1$ at time t. Find $z_{\max} = \max_x f_1(x, t)$ and $z_{\min} = \min_x f_1(x, t)$ at a current time t and put $z_0 = z_{\min} + a(z_{\max} - z_{\min})$ where a, $0 \le a \le 1$, is a constant controlling the filling of the basin with sediments. The curve $\mathscr{L}_2$ is computed at any time t from

the condition

$$\mathscr{L}_2\colon z = f_2^0(x,t) = \begin{cases} z_0 & \text{if } f_1(x,t) < z_0, \\ f_1(x,t) & \text{if } f_1(x,t) > z_0. \end{cases} \tag{14}$$

Hereinafter all variables are dimensionless, unless otherwise stated. The following initial geometry was assumed: the 'free' surface $z = 0.77$ and the heavy ellipse centred at $x = 0$, $z = 0.5$ with vertical and horizontal semi-axes 0.03 and 0.4, respectively. The density above the 'free' surface was 0.0, within sediments 2.5, in the asthenosphere 3.5, and 4.0 in the ellipse. The viscosity was 1.0 above the 'free' surface, 100.0 in the asthenosphere and sediments, and 110.0 within the ellipse. Numerical tests showed that viscosity variation above the 'free' surface

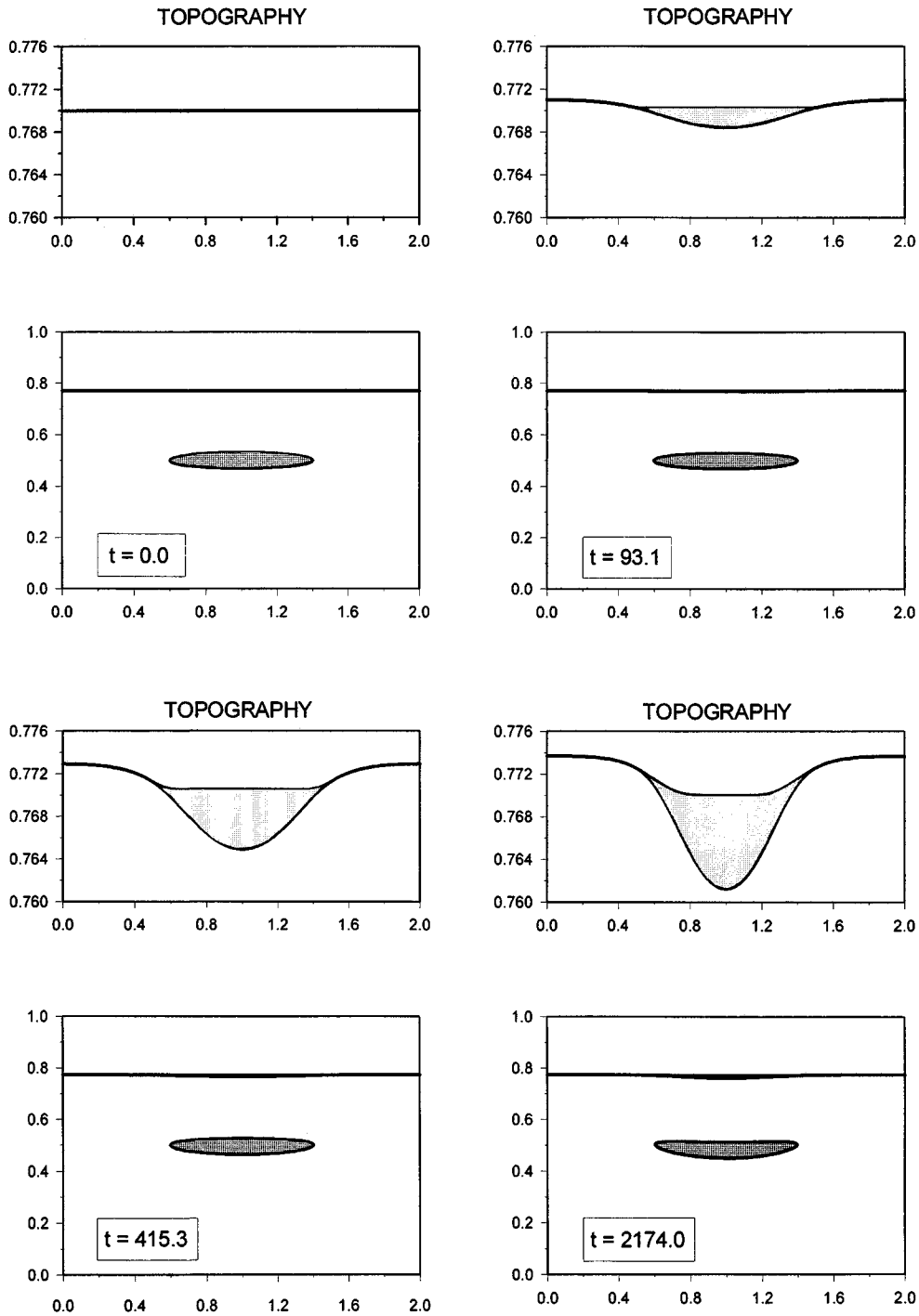

Figure 5. Four phases of sedimentary basin evolution under two effects: the flow produced by a sinking heavy body (shaded) and load due to a sedimentary infill (shaded). Two panels illustrate each phase. The lower panel depicts the position of the 'free' surface and heavy body. The upper panel shows the vicinity of the 'free' surface stretched in the vertical direction to make sedimentary infill and changes of topography clearly visible. We see how the 'free' surface, initially flat, deflects under the actions of the sinking heavy body and of loads due to sediments.

from 1.0 to 10^{-2} resulted in very small changes in numerical solutions. The constant a was taken equal to 0.7: at any time the depression is filled with sediments to 0.7 of its depth. Calculations were made with a rectangular 20 × 25 grid.

Fig. 5 shows four snapshots of a flow at different times. Each snapshot consists of the lower and upper panels. The lower panel depicts the position of the 'free' surface and heavy body. The upper panel shows the vicinity of the 'free' surface stretched in the vertical direction to make sedimentary infill and changes of topography clearly visible. We see how the 'free' surface, initially flat, deflects under the actions of the sinking heavy body and of loads due to sediments.

A test with $a = 0$ (no sediments) leads to similar patterns, but with less subsidence. Fig. 6 shows two subsidence curves: for the cases $a = 0$ (curve 1) and $a = 0.7$ (curve 2). The subsidence was calculated as a depth from the initial position of the 'free' surface to the deepest point of the deflected boundary. We see that sedimentary loads can increase the basement subsidence by a factor of 2 or more.

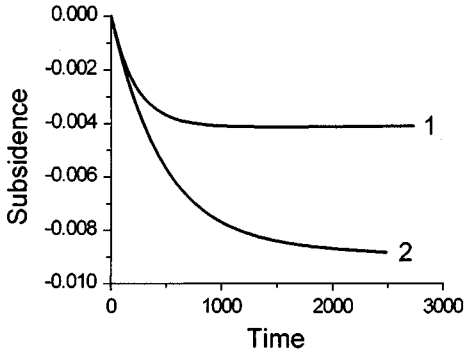

Figure 6. Modelled subsidence curves: in the absence of sedimentary loads (1) and with sediments (2).

Evolution of salt diapirs

Salt diapirism is another process involving viscous flows with material boundaries. Salt tectonics is quite important from the practical point of view, because various types of hydrocarbon traps are closely associated with salt domes (Talbot 1992). Numerical models of salt diapirism were extensively studied by Woidt (1978), Schmeling (1987), Römer & Neugebauer (1991), Poliakov & Podladchikov (1992), Zaleski & Julien (1992), Poliakov *et al.* (1993), Podladchikov, Talbot & Poliakov (1993), Keken *et al.* (1993) and Daudré & Cloetingh (1994).

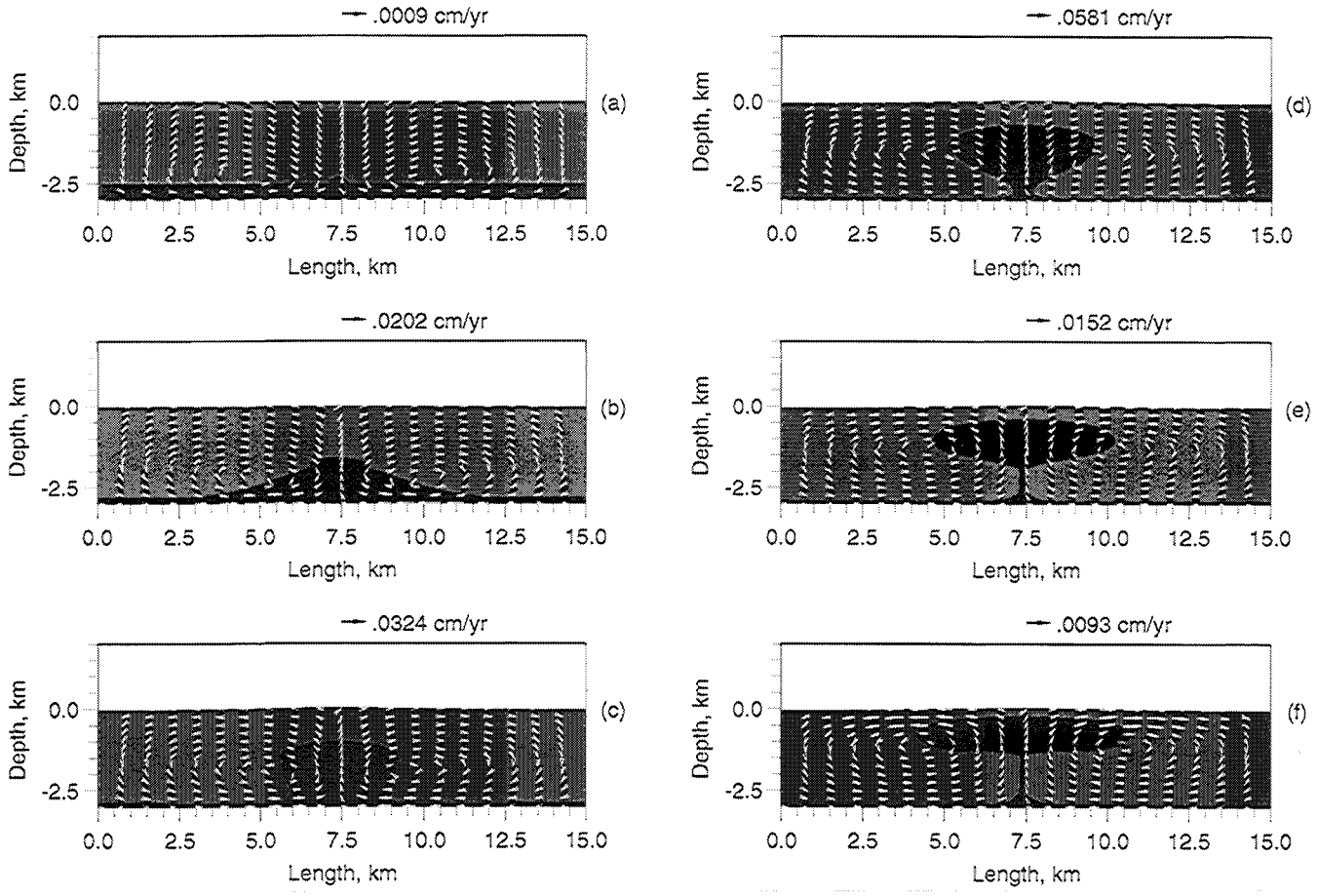

Figure 7. Evolution of salt diapirs, model A. Viscosities and densities are as follows: 10^{20} Pa s and 2.3×10^3 kg m^{-1} (overburden, medium shading) and 10^{18} Pa s and 2.2×10^3 kg m^{-3} (salt, heavy shading). (a) $t = 0$; (b) $t = 27.4$ Ma; (c) $t = 33.7$ Ma; (d) $t = 36.6$ Ma; (e) $t = 41.8$ Ma; (f) $t = 47.1$ Ma. The timescale used is $t^* = \mu^*/(\rho^* gH) = 33.3$ yr, where $\mu^* = 10^{17}$ Pa s and $\rho^* = 2.3 \times 10^3$ kg m^{-3}. Flow velocities are shown by arrows. The velocity scale is given at the top of each figure.

Natural salt structures have various shapes (Jackson & Talbot 1986, Volozh, Groshev & Sinelnikov 1994), which strongly depend on the thickness of the salt layer and that of the surrounding overburden (Schmeling 1987) and on the horizontal gradient of loads due to sediments (Poliakov *et al.* 1993). We present two cases of a salt layer evolution: model A, with the 'balloon on a string' geometry, and model B, where nappes superimposed on the sedimentary overburden lead to asymmetric diapirism. The square model box is 15 km long and 5 km deep. This box is divided into 76×26 rectangular elements in the x and z directions, respectively.

Model A

A salt layer 0.5 km thick at the bottom of the model is covered by a sedimentary overburden 2.5 km thick. The salt/sediment interface is initially perturbed by a peak of cosine shape with amplitude 0.2 km and length 0.57 km. The viscosities and densities are 10^{20} Pa s and 2.3×10^3 kg m^{-3} for the overburden and 10^{18} Pa s and 2.2×10^3 kg m^{-3} for the salt.

Fig. 7 shows the evolution of a diapir evolved from the initial perturbation in 47 Myr. The shapes of salt structures closely agree with classical cases of the Rayleigh–Taylor instability with high viscosity contrasts and a thin lower layer.

Model B

This model presents salt motions in the presence of laterally asymmetrical loading. We feel that nappes of sediments can lead to asymmetrical shapes of salt structures (C. Talbot, personal communication, 1996). The nappe of sediments in model B has maximum thickness 0.99 km, viscosity 10^{20} Pa s and density 1.9×10^3 kg m^{-3}. Fig. 8 shows the evolution of the resultant salt structure. The nappe of sediments was imposed on the overburden with the growing symmetrical diapir (Fig. 8a). The velocity of nappe sinking in the overburden is greater than the rate of diapiric growth. This is clearly seen from velocities presented in Figs 8(a) and (b). Fig. 8(b) demonstrates also how the shape of the diapir becomes slightly asymmetrical. When the nappe attains its equilibrium, the rate of diapiric penetration increases (Fig. 8c). Subsequent phases of diapiric evolution are shown in Figs 8(d) and (e). It is seen that the diapir remains only slightly asymmetric. However, even this minor asymmetry leads to a quite asymmetric shape of the diapir in its subsequent evolution (Fig. 8f).

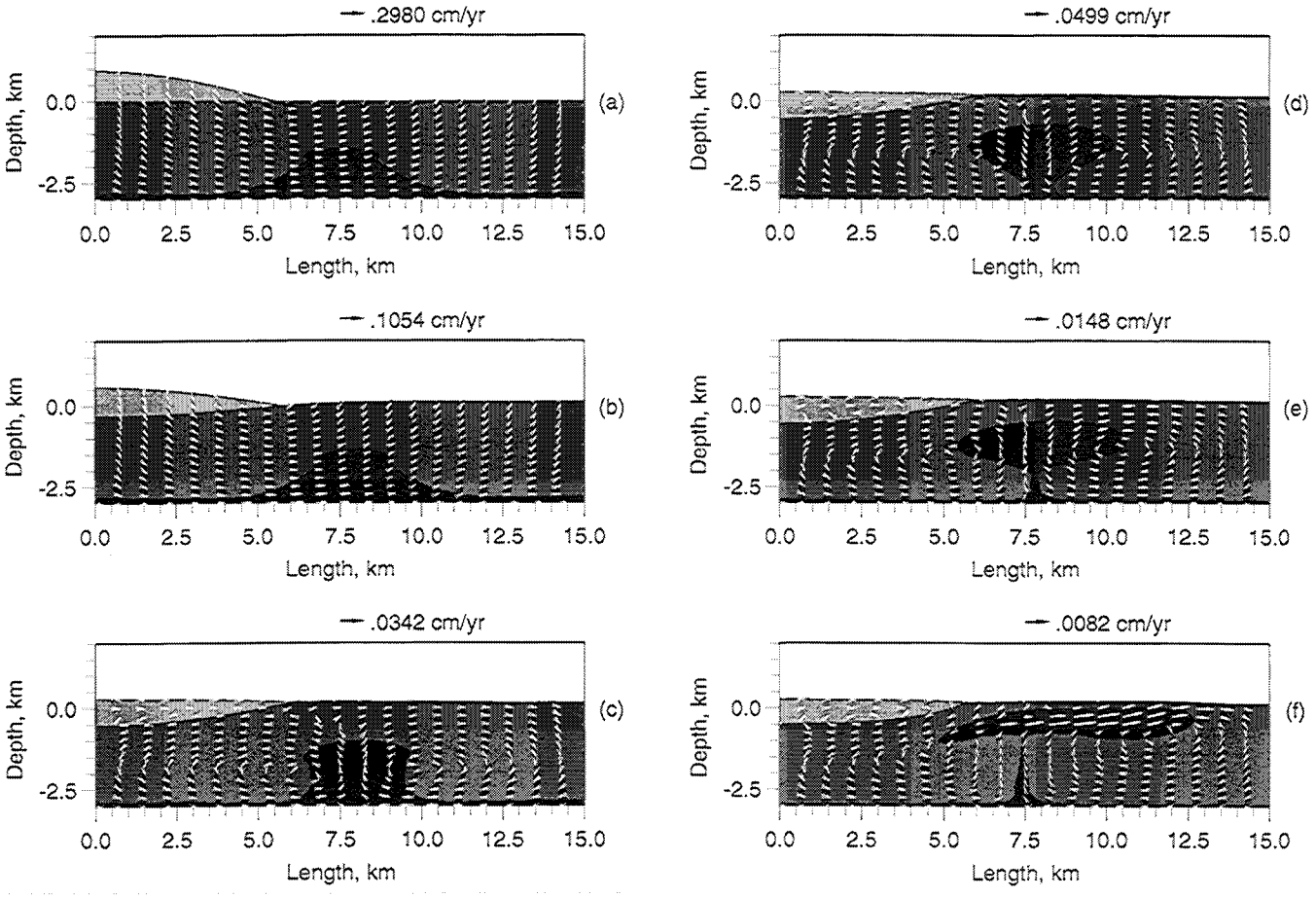

Figure 8. Evolution of salt diapirs under the effect of laterally inhomogeneous sedimentary loads, model B. Three layers are present: salt (heavy shading), overburden (medium shading) and nappe of sediments (light shading). Viscosity and density of sediments' nappe are 10^{20} Pa s and 1.9×10^3 kg m^{-3}. Viscosities and densities of other layers, the timescale and velocity representations are the same as in Fig. 7. (a) $t = 0$; (b) $t = 0.3$ Ma; (c) $t = 3.3$ Ma; (d) $t = 6.4$ Ma; (e) $t = 10.2$ Ma; (f) $t = 30.5$ Ma.

DISCUSSION AND CONCLUSIONS

The method suggested here results in advection of step functions (density and viscosity) free of overshoots and undershoots: the values of ρ_0 and μ_0 in regions bounded by interfaces remain unchanged by definition. However, the method has its limitations, because the difficulty of representing discontinuous changes of physical properties shows up elsewhere. When viscosity is discontinuous across an interface, natural boundary conditions (continuity of stress and velocity) result in discontinuous strain rate, expressed in terms of the second derivatives of the stream function. However, the stream function, being a spline in the assumed approach, must have continuous second derivatives. As a result, the Galerkin method yields the strain rate locally smoothed in the vicinity of the interface. The velocity in the vicinity of the interface is continuous but has a sharp variation. This leads to overshoots and undershoots of the velocity. However, these overshoots and undershoots are not great, because second derivatives of ψ rather than ψ itself are smoothed at the interface.

Numerical tests of the previous method (Naimark & Ismail-Zadeh 1995) show that errors in advected step functions grow with time. A smoothing technique can reduce these errors, but they always tend to increase; they can be treated as perturbations giving rise to new instabilities. Sometimes this leads to erroneous patterns that look like mixing and can result in wrong conclusions. In the suggested method, overshoots and undershoots of velocities do not grow with time; moreover, numerical tests show that these errors tend to decrease on attaining a certain level. From this viewpoint, the present method is more stable than other Eulerian numerical methods involving advection of step functions. Testing of the method for the case of a thin layer shows its advantages.

A numerical model of isostatic adjustment of a layered medium demonstrates a very close agreement with experimental data and results predicted by the linear theory of gravitational instability. The method allows one to take into account the appearance of additional structures bounded by material interfaces, such as nappes of sediments or sedimentary infills.

ACKNOWLEDGMENTS

The authors are grateful to C. Talbot and Yu. Volozh for useful discussions on salt tectonics and to D. Yuen for discussing applications of the method. We would like to thank P. van Keken, A. Malevsky and H. Schmeling for valuable reviews of the initial version of the manuscript and for discussions. ATI is very grateful to R. Nicolich and L. Cernobori, DINMA, University of Trieste, and to E. Aurell and P. Öster, PDC/NADA, Royal Institute of Technology, Stockholm, for computing facilities used to perform a large part of the calculations. ATI was supported by the Swedish Institute and Stockholm University during his stay in PDC/NADA. This research was supported by INTAS (grant 94-1099) and RFBR (grants 96-05-64356, 97-05-65415).

REFERENCES

Biot, M.A. & Ode, H., 1965. Theory of gravity instability with variable overburden and compaction, *Geophysics*, **30**, 213–227.

Chandrasekhar, S., 1968. *Hydrodynamic and Hydromagnetic Stability*, Clarendon Press, Oxford.

Christensen, U., 1982. Phase boundaries in finite amplitude convection, *Geophys. J. R. astr. Soc.*, **68**, 487–497.

Christensen, U.R., 1992. An Eulerian technique for thermomechanical modeling of lithospheric extension, *J. geophys. Res.*, **97**, 2015–2036.

Christensen, U. & Yuen, D., 1984. The interaction of a subducting lithospheric slab with a chemical or phase boundary, *J. geophys. Res.*, **89**, 4389–4402.

Daudré, B. & Cloetingh, S., 1994. Numerical modelling of salt diapirism: influence of the tectonic regime, *Tectonophysics*, **240**, 59–79.

Ismail-Zadeh, A.T., Naimark, B.M. & Lobkovsky, L.I., 1996. Hydrodynamic model of sedimentary basin formation based on development and subsequent phase transformation of a magnetic lens in the upper mantle, in *Computational Seismology and Geodynamics*, Vol. 3, pp. 42–53, ed. Chowdhury, D.K., American Geophysical Union, Washington, DC.

Jackson, M.P.A. & Talbot, C.J., 1986. External shapes, strain rates and dynamics of salt structures, *Geol. Soc. Am. Bull.*, **97**, 305–328.

Jacoby, W.R., 1970. Instability in the upper mantle and global plate movements, *J. geophys. Res.*, **75**, 5671–5680.

Keken, P.E. v., Spiers, C.J., Berg, A.P. v.d. & Muyzert, E.J., 1993. The effective viscosity of rocksalt: implementation of steady-state creep laws in numerical models of salt diapirism, *Tectonophysics*, **225**, 457–476.

Lenardic, A. & Kaula, W.M., 1993. A numerical treatment of geodynamic viscous flow problems involving the advection of material interfaces, *J. geophys. Res.*, **98**, 8243–8260.

Lobkovsky, L.I., Ismail-Zadeh, A.T., Naimark, B.M., Nikishin, A.M. & Cloetingh, S., 1993. Mechanism of crust subsidence and sedimentary basin formation, *Dokl. Rossiyskoy Akad. Nauk*, **330**, 256–260 (in Russian).

Naimark, B.M. & Ismail-Zadeh, A.T., 1994. Gravitational instability of Maxwell upper mantle, in *Computational Seismology and Geodynamics*, Vol. 1, pp. 36–42, ed. Chowdhury, D.K., American Geophysical Union, Washington, DC.

Naimark, B.M. & Ismail-Zadeh, A.T., 1995. Numerical models of subsidence mechanism in intracratonic basin: application to North American basins, *Geophys. J. Int.*, **123**, 149–160.

Naimark, B.M. & Ismail-Zadeh, A.T., 1996. An improved model of subsidence of heavy bodies in the asthenosphere, in *Computational Seismology and Geodynamics*, Vol. 3, pp. 54–62, ed. Chowdhury, D.K., American Geophysical Union, Washington, DC.

Naimark, B.M. & Malevsky, A.V., 1986. Numerical modeling of gravitational instability (in Russian), *Izv. Akad. Nauk SSSR, Fiz. Zemli*, **2**, 44–53.

Naimark, B.M. & Yanovskaya, T.B., 1976. Gravitational stability of viscous incompressible fluid (in Russian), *Comput. Seismol.*, **9**, 149–159.

Podladchikov, Yu., Talbot, C. & Poliakov, A.N.B., 1993. Numerical models of complex diapirs, *Tectonophysics*, **228**, 189–198.

Poliakov, A. & Podladchikov, Yu., 1992. Diapirism and topography, *Geophys. J. Int.*, **109**, 553–564.

Poliakov, A.N.B., van Balen, R., Podladchikov, Yu., Daudre, B., Cloetingh, S. & Talbot, C., 1993. Numerical analysis of how sedimentation and redistribution of surficial sediments affects salt diapirism, *Tectonophysics*, **226**, 199–216.

Ramberg, H., 1968. Instability of layered system in the field of gravity. II, *Phys. Earth planet. Inter.*, **1**, 448–474.

Ribe, N.M. & Christensen, U.R., 1994. Three-dimensional modeling of plume–lithosphere interaction, *J. geophys. Res.*, **99**, 669–682.

Römer, M.-M. & Neugebauer, H.J., 1991. The salt dome problem: a multilayered approach, *J. geophys. Res.*, **96**, 2389–2396.

Schmeling, H., 1987. On the relation between initial conditions and late stages of Rayleigh–Taylor instabilities, *Tectonophysics*, **133**, 65–80.

Schubert, G., Anderson, C. & Goldman, P., 1995. Mantle plume interaction with an endothermic phase change, *J. geophys. Res.*, **100,** 8245–8256.

Talbot, C.J., 1992. Quo vadis tectonophysics? With a pinch of salt!, *J. Geodyn.*, **16,** 1–20.

Volozh, Yu. A., Groshev, V.G. & Sinelnikov, A.V., 1994. The overhangs of the southern Precaspian basin (Kazakhstan): proposals for a genetic classification, *Bull. Center Res. Explor., Elf Aquitaine,* **18,** 19–32.

Woidt, W.-D., 1978. Finite element calculations applied to salt dome analysis, *Tectonophysics,* **50,** 369–386.

Zaleski, S. & Julien, P., 1992. Numerical simulation of Rayleigh–Taylor instability for single and multiple salt diapirs, *Tectonophysics,* **206,** 55–69.

Comput. Math. & Mathl Phys. (2001) **41**, 1428–1444

Numerical Simulation of Three-Dimensional Viscous Flows with Gravitational and Thermal Effects

A.T. Ismail-Zadeh[†], A.I. Korotkii[‡], B.M. Naimark[†] and I.A. Tsepelev[‡]

[†] *International Institute of Earthquake Prediction Theory and Mathematical Geophysics, Russian Academy of Sciences, Warshavskoye sh. 79-2, Moscow 113556, Russia. E-mail: aismail@mitp.ru*

[‡] *Institute of Mathematics and Mechanics, Uralian Branch, Russian Academy of Sciences, S. Kovalevskoy ul. 16, Yekaterinburg 620219, Russia. E-mail: korotkii@imm.uran.ru*

Received 2001 March 15; in original form 2000 August 9

SUMMARY

We consider a three-dimensional model of thermal convection in a highly viscous fluid with temperature-dependent density and viscosity. The model is described by the equations of quasi-steady viscous inhomogeneous incompressible flow, advection equations for density and viscosity, and a heat balance equation. The numerical solution is based on the introduction of a vector velocity potential and on the application of a finite element method with a tricubic-spline basis for computing the potential. The advection equations were solved by the method of characteristics, and the heat equation was solved by a finite-difference method based on a tridiagonal algorithm. A new two-component representation (in some cases, a one-component representation) was found for the velocity potential, which allowed to substantially reduce computational costs. The numerical algorithms employed were designed to be implemented on parallel computers. The principal results of the study are summarized as follows: a numerical method is developed for simultaneous solution of the Stokes flow equation, heat balance equation, and advection equations for physical parameters of the fluid; it is shown that computational costs can be reduced by decreasing the dimensionality of the vector velocity potential; a model example is computed and computational performance is analyzed.

Key words: Thermal convection, Diapirism, Eulerian FEM, Galerkin-spline approach

1 INTRODUCTION

We consider the numerical simulation of three-dimensional, inhomogeneous, highly viscous, incompressible flows under gravitational and thermal effects. Problems of this kind frequently arise in geophysics when various processes taking place in the earth's interior are to be modeled (McKenzie et al. 1974; Turcotte & Schubert 1982; Ismail-Zadeh et al. 1996; Rykov & Trubitsyn 1996). A particular problem of interest is the simulation of evolution of slat and other evaporite structures in the crust, development of sedimentary basins, thermally driven convection in the earth's mantle, and other processes. Three-dimensional numerical models of geophysical processes provide a basis for the most realistic simulations, but entail high computational complexity, which can be dealt with only on high-performance computers. Therefore, solution of three-dimensional problems must rely on highly efficient computational methods. Moreover, their numerical implementation frequently requires special procedures consistent with the architecture of the computer employed.

In geophysical problems, three-dimensional simulations of thermally driven convection in a rectangular domain have been performed by various investigators both for constant viscosity (e.g., see Cserepes et al. 1988; Houseman 1988; Travis et al.1990) and for variable viscosity (e.g., Frick et al. 1983; Busse & Frick 1985; Christensen & Harder 1991; Ogawa et al. 1991; Tackley 1993; Rykov & Trubitsyn 1996; Trompert & Hansen 1996). They were based on the use of finite-difference, spectral, and multigrid methods.

In this paper, we propose methods and algorithms that can be used in numerical simulations of the problems mentioned above on modern parallel computers. The numerical simulation of the problem analyzed here relies on general equations of inhomogeneous viscous incompressible flow: a momentum equation, a heat balance equation, transport equations for physical parameters of the fluid, and an equation of state. These equations are modified and simplified by taking into account certain fluid properties and flow characteristics (high viscosity and low velocity). We eliminate the convective terms from the equation of motion (since the Reynolds numbers of typical flows under study are very low) to reduce it to the corresponding Stokes quasi-steady flow equation. We introduce a vector velocity potential and transform the governing equations, applying the curl operator to eliminate the incompressibility condition and pressure. The vector velocity potential is approximated by a linear combination of suitable basis functions consisting of certain localized tricubic splines. The approximation is determined from an appropriate variational equation corresponding to the Stokes flow equation. We write out a system of linear algebraic equations for the approximation coefficients, which has a high dimension even for relatively coarse grid discretizations of the computational domain. This system is nonsingular by virtue of a special choice of basis functions in the finite element method, but the condition number of its matrix tends to infinity as the computational grid is condensed. Such systems of equations must be solved repeatedly, because their coefficients and right-hand sides are updated at each time step. This leads to certain conditions to be satisfied by the choice of solution procedures, and parallel algorithms prove to be definitely advantageous since test computations have shown that a greater part of the CPU time resources consumed is required to solve the systems of equations in question. Density and viscosity are found from the relevant first-order partial differential equations (advection equations) or from the ordinary differential equations for the characteristics of the advection equations (with subsequent transfer of the initial density and viscosity along the characteristics). Temperature is determined from the heat balance equation by a finite-difference method. The well-posedness and solvability of the corresponding two-dimensional boundary value problems were analyzed by Naimark (1986, 1988).

Numerical analysis of problems of this type is difficult to perform because of the high dimensionality of finite-difference approximations. Considerable progress achieved in dealing with this difficulty became possible by constructing a special set of basis functions in the finite element method and using a two-component representation of the vector velocity potential proposed here. As a consequence, we managed to reduce computational costs and obtain adequate qualitative and quantitative results for relatively low-dimensional discretizations.

In what follows, we state the problem, restate it in a more tractable form, describe the overall computational procedure and some of its details, and present the results obtained by computing a model example reflecting some essential features of the real process.

2 DESCRIPTION OF THE MODEL AND STATEMENT OF THE PROBLEM

In a spatial domain Ω we consider an inhomogeneous viscous incompressible flow in the presence of a gravity field and a temperature gradient. We describe the flow in terms of Eulerian variables. In Cartesian coordinates, the flow is governed by the following equations (Chandrasekhar 1968; Landau & Lifshitz 1987):

the momentum (Navier–Stokes) equations

$$\rho\left(\frac{\partial\vec{u}}{\partial t}+<\vec{u},\nabla>\vec{u}\right)=-\nabla p+\mathrm{div}\,(\,\mu\,e_{ij}\,)+\vec{F}, \qquad (1)$$

the incompressibility condition

$$\mathrm{div}\;\vec{u}=0, \qquad (2)$$

the heat balance equation

$$\frac{\partial}{\partial t}(\rho cT)+<\vec{u},\nabla(\rho cT)>=\mathrm{div}\,(\,k\;\nabla T)+\mu\Phi+\rho Q, \qquad (3)$$

the equation of state

$$\rho(t,x)=\rho_*(t,x)(1-\alpha(T(t,x)-T_0)), \qquad (4)$$

the rheological equation

$$\mu(t,x)=\mu_*(t,x)\exp\left(\frac{E+\rho_* g x_3 V}{RT}-\frac{E_0+\rho_0 g_0 l_0 V_0}{RT_0}\right), \qquad (5)$$

and the advection equations for thermally unperturbed density and viscosity

$$\frac{\partial\rho_*}{\partial t}+<\nabla\rho_*,\vec{u}>=0,\quad \frac{\partial\mu_*}{\partial t}+<\nabla\mu_*,\vec{u}>=0. \qquad (6)$$

Equations (1)–(6) contain the following variables and parameters: time t; a spatial point x with Cartesian coordinates (x_1,x_2,x_3); velocity vector $\vec{u}=(u_1(t,x),u_2(t,x),u_3(t,x))$; pressure $p=p(t,x)$; absolute

temperature $T = T(t,x)$; density $\rho = \rho(t,x)$; viscosity $\mu = \mu(t,x)$; thermally unperturbed density $\rho_* = \rho_*(t,x)$; thermally unperturbed viscosity $\mu_* = \mu_*(t,x)$; acceleration due to gravity g; universal gad constant R; external body force (gravity) per unit volume $\vec{F} = -g\rho\vec{e}_3 = (0,0,-g\rho)$; unit basis vector $\vec{e}_3$ for the Ox_3 axis; specific heat c; heat conductivity k; coefficient of thermal expansion α; activation energy E; activation volume V; a dissipation function $\Phi = \Phi(t,x)$ representing the rate of heat production due to internal friction; the rate of heat production per unit volume due to nonviscous heat sources $Q = Q(t,x)$; and reference physical parameters ρ_0, g_0, l_0, E_0 V_0, and T_0 defined below.

Here, ∇, div , and e_{ij} denote the gradient operator, divergence operator, and strain rate tensor $e_{ij} = e_{ij}(\vec{u}) = \partial u_i/\partial x_j + \partial u_j/\partial x_i$, respectively

$$\text{div}\ (\mu e_{ij})$$

$$= \left(\sum_{m=1}^{3} \frac{\partial\ (\mu e_{m1})}{\partial x_m}, \sum_{m=1}^{3} \frac{\partial\ (\mu e_{m2})}{\partial x_m}, \sum_{m=1}^{3} \frac{\partial\ (\mu e_{m3})}{\partial x_m} \right),$$

$$\Phi = \frac{1}{2} \sum_{i=1}^{3} \sum_{j=1}^{3} (e_{ij})^2.$$

Equations (1)–(6) make up a closed set of equations that determine the unknown u_1, u_2, u_3, T, p, ρ_*, and μ_* as functions of independent variables t and x. Appropriate initial and boundary conditions for the desired functions are formulated below.

Thus, we seek functions $u_1 = u_1(t,x)$, $u_2 = u_2(t,x)$, $u_3 = u_3(t,x)$, $T = T(t,x)$, $p = p(t,x)$, $\rho = \rho(t,x)$, and $\mu = \mu(t,x)$ that satisfy both Eqs. (1)–(6) in a domain Ω at $t \geq t_0$ (where t_0 is an initial time) and prescribed boundary and initial conditions.

3 TRANSFORMATION OF THE PROBLEM

Equations (1)–(6) can be simplified by changing to dimensionless quantities and taking into consideration the characteristic values of these quantities. As characteristic values of parameters and variables, we introduce the following reference quantities: length l_0, density ρ_0, viscosity μ_0, temperature T_0, specific heat c_0, heat conductivity k_0, the rate of heat production per unit mass Q_0, the acceleration due to gravity g_0, coefficient of thermal expansion α_0, activation energy E_0, activation volume V_0, thermal diffusivity $æ_0 = k_0/(\rho_0 c_0)$, time $t_0 = l_0^2/æ_0$, velocity $u_0 = l_0/t_0$, and pressure $p_0 = g_0\rho_0 l_0$.

We define new dimensionless variables and parameters (denoted by prime) as follows: $t = t' \cdot t_0$, $x = x' \cdot l_0$, $\vec{u} = (\vec{u})' \cdot u_0$, $T = T' \cdot T_0$, $p = p' \cdot p_0$, $\rho = \rho' \cdot \rho_0$, $\rho_* = \rho'_* \cdot \rho_0$, $\mu = \mu' \cdot \mu_0$, $\mu_* = \mu'_* \cdot \mu_0$, $g = g' \cdot g_0$, $\alpha = \alpha' \cdot \alpha_0$, $k = k' \cdot k_0$, $E = E' \cdot E_0$, $V = V' \cdot V_0$, $c = c' \cdot c_0$, and $Q = Q' \cdot Q_0$.

After the change of variables the governing equations have the form

$$\text{Fr} \cdot \rho \left(\frac{\partial \vec{u}}{\partial t} + < \vec{u}, \nabla > \vec{u} \right)$$

$$= -\nabla p + \frac{1}{\text{La}} \cdot \text{div}\ (\mu\, e_{ij}) + \vec{F},$$

$$\text{div}\ \vec{u} = 0, \quad \frac{\partial}{\partial t}(\rho c T) + < \vec{u}, \nabla(\rho c T) >$$

$$= \text{div}\ (k\ \nabla T) + \text{Di} \cdot \mu\Phi + \text{He} \cdot \rho Q,$$

$$\rho(t,x) = \rho_*(t,x)(1 - \alpha\alpha_0 T_0 (T(t,x) - 1)),$$

$$\mu(t,x) = \mu_*(t,x) \exp\left(\frac{E_0 E + \rho_* \rho_0 g g_0 x_3 l_0 V_0 V}{R T T_0} \right.$$

$$\left. - \frac{E_0 + \rho_0 g_0 l_0 V_0}{R T_0} \right),$$

$$\frac{\partial \rho_*}{\partial t} + < \nabla \rho_*, \vec{u} >= 0, \quad \frac{\partial \mu_*}{\partial t} + < \nabla \mu_*, \vec{u} >= 0.$$

These equations are written in terms of dimensionless variables and parameters. Hereinafter, we omit the primes to simplify notation, which is thus made similar to the original dimensional notation. The equations contain the following dimensionless parameters:

$$\text{Fr} = \frac{æ_0^2}{g_0 l_0^3} = \frac{u_0^2}{g_0 l_0}, \quad \text{La} = \frac{\rho_0 g_0 l_0^3}{\mu_0 æ_0},$$

$$\text{Di} = \frac{\mu_0 æ_0}{c_0 \rho_0 T_0 l_0^2}, \quad \text{He} = \frac{l_0^2 Q_0}{æ_0 T_0 c_0}.$$

Here, Fr is the Froude number, Di is a parameter characterizing the rate of heat production due to the conversion of mechanical energy into internal energy through viscous friction, and He is a parameter characterizing the heat production due to other internal sources. Also we use $\text{Ra} = \alpha_0 T_0 \text{La}$, the Rayleigh number. Let us estimate these parameters by using the following typical values of the physical parameters for the uppermost layers of the Earth: $g_0 = 9.8$ m·s^{-2}; $\alpha_0 = 10^{-5}$ K^{-1}; $\rho_0 = 2.2 \times 10^3$ kg·m^{-3}; $\mu_0 = 10^{18}$ Pa·s; $l_0 = 5 \times 10^3$ m; $k_0 = 3$ J ·K^{-1}·m^{-1} ·s^{-1}; $c_0 = 1250$ J ·kg^{-1}·K^{-1}; $T_0 = 673$ K; $E_0 = 2 \times 10^4$ J ·mol^{-1}; $V_0 = 4 \times 10^{-6}$ m^3·mol^{-1}; $R = 8.3$ J ·mol^{-1}·K^{-1}; $Q_0 = 0$ J ·kg^{-1}·s^{-1}. As a result, we obtain $\text{Fr} = 0.95 \times 10^{-24}$, $\text{La} = 2.52 \times 10^3$, $\text{Ra} = 16.96$, $\text{Di} = 0.24 \times 10^{-4}$, and $\text{He} = 0.27 \times 10^8 \cdot Q_0 = 0$. The effective values of these parameters can substantially differ from those listed here, because the problem is solved for the density ρ and viscosity μ calculated by using formulas (4) and (5) or their dimensionless counterparts. The resulting effective value of the Rayleigh number is sufficiently high to be indicative of an unstable flow. Thus, since the geodynamical processes are slow and the inertia-to-gravity force ratio is a small quantity, one can

set Fr = 0 and drop the terms on the left-hand side of the Navier–Stokes equations.

We note that the parameters c, k, α, and æ, characterizing properties of the fluid, are advected by fluid particles in the same manner as the thermally unperturbed density and viscosity. Therefore, these parameters should satisfy the following equation:

$$\frac{\partial [\,\cdot\,]}{\partial t} + < \nabla[\,\cdot\,], \vec{u} >= 0.$$

These parameters may be complicated functions of temperature, pressure, and other flow variables. To simplify analysis and avoid unnecessary solution of additional equations, we assumed that c, k, α, and æ are constant parameters. Accordingly, transport equations for these parameters were not included in the set of relations that determine the flow dynamics. Assuming also that the gravitational acceleration, activation energy, and activation volume are constant parameters, we set $c = 1$, $k = 1$, $\alpha = 1$, æ $= 1$, $g = 1$, $E = 1$, and $V = 1$ in the governing equations. The heat equation was considered in the Boussinesq approximation. The simplifications and assumptions introduced above lead to the following simplified system of equations for the desired dimensionless flow variables:

$$\mathrm{La} \cdot \nabla p = \mathrm{div}\ (\ \mu\ e_{ij}\ ) - \mathrm{La} \cdot \rho\ \vec{e}_3, \tag{7}$$

$$\mathrm{div}\ \vec{u} = 0, \tag{8}$$

$$\frac{\partial}{\partial t}(\rho_* T) + < \vec{u}, \nabla(\rho_* T) >= \Delta T + \mathrm{Di} \cdot \mu\Phi, \tag{9}$$

$$\rho(t,x) = \rho_*(t,x)(1 - \alpha_0 T_0 (T(t,x) - 1)), \tag{10}$$

$$\mu(t,x) = \mu_*(t,x)\exp\Big(\frac{E_0 + \rho_* x_3 p_0 V_0}{RTT_0} - \frac{E_0 + p_0 V_0}{RT_0}\Big), \tag{11}$$

$$\frac{\partial \rho_*}{\partial t} + < \nabla \rho_*, \vec{u} >= 0, \quad \frac{\partial \mu_*}{\partial t} + < \nabla \mu_*, \vec{u} >= 0. \tag{12}$$

To eliminate the incompressibility condition div $\vec{u} = 0$ and pressure p, we define the vector potential $\vec{\psi} = (\psi_1, \psi_2, \psi_3)$ by the relation $\vec{u} = \mathrm{curl}\vec{\psi}$ and apply the curl operator to Eq. (7). Using the identities $\mathrm{curl}(\nabla p) = 0$ and $\mathrm{div}\ (\mathrm{curl}\vec{\psi}) = 0$, we derive the following equations from (7) and (8):

$$\sum_{i=1}^{3}\Big[\frac{\partial^2(\mu\ e_{i3})}{\partial x_2 \partial x_i} - \frac{\partial^2(\mu\ e_{i2})}{\partial x_3 \partial x_i}\Big] = \tag{13}$$

$$\Big(\mathrm{La}(1 + \alpha_0 T_0) - \mathrm{Ra}T\Big)\frac{\partial \rho_*}{\partial x_2} - \mathrm{Ra}\rho_* \frac{\partial T}{\partial x_2},$$

$$\sum_{i=1}^{3}\Big[\frac{\partial^2(\mu\ e_{i3})}{\partial x_1 \partial x_i} - \frac{\partial^2(\mu\ e_{i1})}{\partial x_3 \partial x_i}\Big] = \tag{14}$$

$$\Big(\mathrm{La}(1 + \alpha_0 T_0) - \mathrm{Ra}T\Big)\frac{\partial \rho_*}{\partial x_1} - \mathrm{Ra}\rho_* \frac{\partial T}{\partial x_1},$$

$$\sum_{i=1}^{3}\Big[\frac{\partial^2(\mu\ e_{i2})}{\partial x_1 \partial x_i} - \frac{\partial^2(\mu\ e_{i1})}{\partial x_2 \partial x_i}\Big] = 0. \tag{15}$$

Pressure p can be determined from (7) up to a constant. The components of velocity vector $\vec{u} = (u_1, u_2, u_3)$ can be found from the equation $\vec{u} = \mathrm{rot}\ \vec{\psi}$ as

$$u_1 = \frac{\partial \psi_3}{\partial x_2} - \frac{\partial \psi_2}{\partial x_3},\ u_2 = \frac{\partial \psi_1}{\partial x_3} - \frac{\partial \psi_3}{\partial x_1},\ u_3 = \frac{\partial \psi_2}{\partial x_1} - \frac{\partial \psi_1}{\partial x_2}. \tag{16}$$

Equations (9)–(15) should be satisfied within the domain Ω at $t \geq t_0$. The functions ψ_1, ψ_2, ψ_3, and T should satisfy the conditions at the boundary Γ of the domain Ω, and the functions T, ρ_*, and μ_* should satisfy the initial conditions. We now proceed to formulating these conditions.

4 BOUNDARY AND INITIAL CONDITIONS

We set the initial time at zero: $t_0 = 0$. For simplicity, the domain Ω is supposed to be a parallelepiped: $\Omega = (0, l_1) \times (0, l_2) \times (0, l_3)$. On the boundary Γ of Ω, which consists of the faces $\Gamma(x_i = 0)$ and $\Gamma(x_i = l_i)$ $(i = 1, 2, 3)$, we set impermeability conditions with either perfect slip or no-slip conditions.

In the case of impermeability conditions with perfect slip, the velocity vector satisfies the following conditions at any $t \geq 0$:

$$\partial \vec{u}_\tau / \partial \vec{n} = 0, \quad < \vec{u}, \vec{n} >= 0 \quad \text{at } \Gamma.$$

Here, $\vec{n}$ is the outward unit normal vector at a point on the boundary Γ, and $\vec{u}_\tau$ is the projection of the velocity vector onto the tangent plane at the same point on Γ.

In the case of no-slip conditions, the velocity vector satisfies the following condition at any $t \geq 0$:

$$\vec{u} = 0 \quad \text{at } \Gamma.$$

Using the equation $\vec{u} = \mathrm{curl}\vec{\psi}$, we represent the corresponding natural boundary conditions in terms of $\vec{\psi}$. In the case of impermeability conditions with perfect slip, we have

$$\Gamma(x_1 = 0, x_1 = l_1): \ \frac{\partial \psi_3}{\partial x_2} - \frac{\partial \psi_2}{\partial x_3} = 0,$$

$$\frac{\partial^2 \psi_1}{\partial x_1 \partial x_3} - \frac{\partial^2 \psi_3}{\partial x_1 \partial x_1} = 0, \ \frac{\partial^2 \psi_2}{\partial x_1 \partial x_1} - \frac{\partial^2 \psi_1}{\partial x_1 \partial x_2} = 0;$$

$$\Gamma(x_2 = 0, x_2 = l_2): \ \frac{\partial \psi_1}{\partial x_3} - \frac{\partial \psi_3}{\partial x_1} = 0,$$

$$\frac{\partial^2 \psi_3}{\partial x_2 \partial x_2} - \frac{\partial^2 \psi_2}{\partial x_2 \partial x_3} = 0, \ \frac{\partial^2 \psi_2}{\partial x_1 \partial x_2} - \frac{\partial^2 \psi_1}{\partial x_2 \partial x_2} = 0;$$

$$\Gamma(x_3 = 0, x_3 = l_3): \ \frac{\partial \psi_2}{\partial x_1} - \frac{\partial \psi_1}{\partial x_2} = 0,$$

$$\frac{\partial^2 \psi_3}{\partial x_2 \partial x_3} - \frac{\partial^2 \psi_2}{\partial x_3 \partial x_3} = 0, \ \frac{\partial^2 \psi_1}{\partial x_3 \partial x_3} - \frac{\partial^2 \psi_3}{\partial x_1 \partial x_3} = 0.$$

In the case of no-slip conditions, we have

$$\Gamma(x_1 = 0, x_1 = l_1): \ \frac{\partial \psi_3}{\partial x_2} - \frac{\partial \psi_2}{\partial x_3} = 0,$$

$$\frac{\partial\psi_1}{\partial x_3}-\frac{\partial\psi_3}{\partial x_1}=0,\quad \frac{\partial\psi_2}{\partial x_1}-\frac{\partial\psi_1}{\partial x_2}=0;$$

$$\Gamma(x_2=0,x_2=l_2):\ \frac{\partial\psi_3}{\partial x_2}-\frac{\partial\psi_2}{\partial x_3}=0,$$

$$\frac{\partial\psi_1}{\partial x_3}-\frac{\partial\psi_3}{\partial x_1}=0,\quad \frac{\partial\psi_2}{\partial x_1}-\frac{\partial\psi_1}{\partial x_2}=0;$$

$$\Gamma(x_3=0,x_3=l_3):\ \frac{\partial\psi_3}{\partial x_2}-\frac{\partial\psi_2}{\partial x_3}=0,$$

$$\frac{\partial\psi_1}{\partial x_3}-\frac{\partial\psi_3}{\partial x_1}=0,\quad \frac{\partial\psi_2}{\partial x_1}-\frac{\partial\psi_1}{\partial x_2}=0.$$

However, we consider somewhat less specific and more restrictive boundary conditions for $\vec{\psi}$ to simplify natural boundary conditions in the case when the variables in $\vec{\psi}$ are separated as follows:

$$\psi_i=\psi_i(x_1,x_2,x_3)=\psi_1^{(i)}(x_1)\cdot\psi_2^{(i)}(x_2)\cdot\psi_3^{(i)}(x_3),$$

$$i=1,2,3.$$

In the case of impermeability conditions with perfect slip, the following more restrictive conditions are set:

$$\Gamma(x_1=0,x_1=l_1):\quad \psi_2=\psi_3=0,$$

$$\frac{\partial\psi_1}{\partial x_1}=0,\quad \frac{\partial^2\psi_2}{\partial x_1^2}=\frac{\partial^2\psi_3}{\partial x_1^2}=0;$$

$$\Gamma(x_2=0,x_2=l_2):\quad \psi_1=\psi_3=0,$$

$$\frac{\partial\psi_2}{\partial x_2}=0,\quad \frac{\partial^2\psi_1}{\partial x_2^2}=\frac{\partial^2\psi_3}{\partial x_2^2}=0;$$

$$\Gamma(x_3=0,x_3=l_3):\quad \psi_1=\psi_2=0,$$

$$\frac{\partial\psi_3}{\partial x_3}=0,\quad \frac{\partial^2\psi_1}{\partial x_3^2}=\frac{\partial^2\psi_2}{\partial x_3^2}=0.$$

In the case of no-slip conditions, we set the following conditions:

$$\Gamma(x_1=0,x_1=l_1):\psi_1=\psi_2=\psi_3=0,\ \frac{\partial\psi_2}{\partial x_1}=\frac{\partial\psi_3}{\partial x_1}=0;$$

$$\Gamma(x_2=0,x_2=l_2):\psi_1=\psi_2=\psi_3=0,\ \frac{\partial\psi_1}{\partial x_2}=\frac{\partial\psi_3}{\partial x_2}=0;$$

$$\Gamma(x_3=0,x_3=l_3):\psi_1=\psi_2=\psi_3=0,\ \frac{\partial\psi_1}{\partial x_3}=\frac{\partial\psi_2}{\partial x_3}=0.$$

For the temperature on the side faces on Ω, we set zero heat flux conditions (as in a homogeneous Neumann problem). On the top and bottom faces of Ω, the following conditions for temperature are prescribed (as in a nonhomogeneous Dirichlet problem):

$$\Gamma(x_1=0,x_1=l_1):\quad \partial T/\partial x_1=0,\quad t\geq 0;$$

$$\Gamma(x_2=0,x_2=l_2):\quad \partial T/\partial x_2=0,\quad t\geq 0;$$

$$\Gamma(x_3=0):\quad T(t,x_1,x_2,0)=T_1(t,x_1,x_2),\quad t\geq 0;$$

$$\Gamma(x_3=l_3):\quad T(t,x_1,x_2,l_3)=T_2(t,x_1,x_2),\quad t\geq 0.$$

The initial conditions for temperature, density, and viscosity are set as follows:

$$T(0,x)=T_*^0(x),\quad \rho_*(0,x)=\rho_*^0(x),$$

$$\mu_*(0,x)=\mu_*^0(x),\quad x\in\Omega.$$

Here, the prescribed functions T_*^0, ρ_*^0, and μ_*^0 define the temperature and thermally unperturbed density and viscosity at the initial time.

Equations (7)–(12) combined with the boundary and initial conditions uniquely determine the unknown functions u_1, u_2, u_3, T, ρ, and μ within Ω at any $t\geq 0$. Equations (13)–(15) (with prescribed functions T, ρ_*, and μ_*) do not uniquely determine ψ_1, ψ_2, and ψ_3 under boundary conditions of any form. This is explained by the fact that $\vec{u}$ can be expressed in terms of the corresponding vector potential $\vec{\psi}$ only up to the gradient of an arbitrary differentiable scalar function φ, because $\vec{u}=\mathrm{curl}\vec{\psi}=\mathrm{curl}(\vec{\psi}+\nabla\varphi)$, which implies that $\vec{u}=\mathrm{curl}\vec{\psi}_1$, $\vec{u}=\mathrm{curl}\vec{\psi}_2$, то $\vec{\psi}_1=\vec{\psi}_2+\nabla\varphi$. When a potential $\vec{\psi}$ satisfies these relations, the potential $\vec{\psi}+\nabla\varphi$, where φ is an arbitrary sufficiently smooth function of $x\in\Omega$ with a compact support in Ω, satisfies these relations as well. Since φ is a compactly supported function on Ω, the gradient $\nabla\varphi$ does not contribute to the boundary conditions for $\vec{\psi}$. In particular, this implies that Eqs. (9)–(15) combined with the boundary and initial conditions do not uniquely determine the unknown functions ψ_1, ψ_2, and ψ_3, whereas the unknown functions T, ρ_*, and μ_* (and, therefore, T, ρ, and μ) are uniquely determined within Ω at any $t\geq 0$. For our purposes, any potential found by solving the equations above is suitable, because the same velocity field is obtained.

5 VARIATIONAL EQUATION OF THE PROBLEM

To apply a finite element method, we replace Eqs. (13)–(15) with an equivalent variational equation. We multiply Eqs. (13)–(15) by the components ω_i of a test vector function $\vec{\omega}$ satisfying the conditions set for the vector function $\vec{\psi}$. Performing these operations and using the boundary conditions for the desired and test vector functions, we obtain the variational equation

$$\int_\Omega \mu\cdot(2e_{11}\tilde{e}_{11}+2e_{22}\tilde{e}_{22}+2e_{33}\tilde{e}_{33}+e_{12}\tilde{e}_{12}$$

$$+e_{13}\tilde{e}_{13}+e_{23}\tilde{e}_{23})dx=-\int_\Omega La\rho w_3 dx,$$

which can be represented as

$$E(\vec{\psi},\vec{\omega})=L(\vec{\omega}) \tag{17}$$

for any arbitrary admissible $\vec{\omega}=(\omega_1,\omega_2,\omega_3)$. Here, $E(\vec{\psi},\vec{\omega})$ and $L(\vec{\omega})$ denote the corresponding bilinear and linear forms. The expressions for $\tilde{e}_{ij}$ in terms of $\vec{\omega}$ are identical to the expressions for e_{ij} in terms of $\vec{\psi}$.

The bilinear form $E(\vec{\psi},\vec{\omega})$ is symmetric, $E(\vec{\psi},\ \vec{\omega}) = E(\vec{\omega},\ \vec{\psi})$ for any arbitrary admissible $\vec{\psi}$ and $\vec{\omega}$. Moreover, it is nonnegative, $E(\vec{\omega},\vec{\omega}) \geq 0$ for any arbitrary admissible $\vec{\omega}$. However, it is not positive definite; otherwise, the potential would be uniquely defined, which is not the case here, as shown above. Thus, the problem is reduced to computing the functions $\psi_1 = \psi_1(t,x)$, $\psi_2 = \psi_2(t,x)$, $\psi_3 = \psi_3(t,x)$, $T = T(t,x)$, $\rho = \rho(t,x)$, and $\mu = \mu(t,x)$ that satisfy Eqs. (9)–(15) in the domain Ω at $t \geq 0$ (or the variational equation (17) combined with Eqs. (9)–(12)), supplemented with the boundary and initial conditions formulated above.

6 TWO-COMPONENT REPRESENTATION OF THE VECTOR POTENTIAL

Let us discuss the possibility of reducing the number of functions to be computed by reducing the number of required components of the vector potential $\vec{\psi}$. Since numerical solution of the problem involves repeated computation of the flow velocity field (at different times t) based on the corresponding current potential field, and the problem under analysis is three-dimensional, the reduction of the number of computed components of $\vec{\psi}$ (say, from three to two) would result in a substantial economy of computing resources. This is a feasible task, because, as noted above, the vector potential is determined by the velocity field except for an additive gradient of a scalar function. Therefore, one can try to use the freedom in choosing a vector potential to accomplish this task.

We show here that, for a wide class of problems, it can be assumed a priori that $\psi_3 = 0$ in the required vector velocity potential $\vec{\psi}$. To make this possible, we should find cases where the vector velocity field $\vec{u}$ admits the representation

$$\vec{u} = \mathrm{curl}\vec{\psi}, \quad \vec{\psi} = (\psi_1, \psi_2, \psi_3), \quad \psi_3 = 0, \tag{18}$$

where the two-component potential $\vec{\psi} = (\psi_1, \psi_2, 0)$ satisfies certain boundary conditions. The existence of such a representation would imply that the vector velocity potential could be sought in the two-component form and could be determined by solving either a simplified version of Eqs. (13)–(15) or a simplified variational equation derived from (17) under appropriately simplified boundary conditions with $\psi_3 = 0$. In what follows, we indicate some cases when this is possible.

Omitting a detailed analysis, we note the following fact verifiable by direct computation: for any sufficiently smooth vector field @u satisfying only the incompressibility condition and an impermeability condition with either perfect slip or a no-slip condition, there exists a sufficiently smooth vector field $\vec{\psi}$ that satisfies Eqs. (18) and the corresponding natural boundary conditions equivalent to impermeability with either perfect slip or no-slip. As an example of such a $\vec{\psi}$, we consider the field defined by the following simple expressions:

$$\psi_1 = \psi_1(t,x_1,x_2,x_3) = \int_0^{x_3} u_2(t,x_1,x_2,\xi)\, d\xi + \frac{\partial\varphi}{\partial x_1}\,, \tag{19}$$

$$\psi_2 = \psi_2(t,x_1,x_2,x_3) = -\int_0^{x_3} u_1(t,x_1,x_2,\xi)\, d\xi + \frac{\partial\varphi}{\partial x_2}\,, \tag{20}$$

$$\psi_3 = \psi_3(t,x_1,x_2,x_3) = 0\,, \tag{21}$$

where $\varphi = \varphi(t,x_1,x_2)$ is an arbitrary sufficiently smooth scalar function with a compact support in the rectangular domain $(0,l_1) \times (0,l_2)$ (the variable t is treated here as a parameter). However, as mentioned above, it is more convenient from a computational perspective to deal with more restrictive boundary conditions for the velocity potential, because suitable basis functions are much easier to construct under such conditions in the finite element method to be used here in the approximate computation of the potential. In the analysis below, we use basis functions constructed from tricubic splines.

Now, let us explore the applicability of representation (18) under more restrictive boundary conditions for $\vec{\psi}$. We begin with the case of more restrictive impermeability conditions with perfect slip. We show here that the scalar function φ in (19)–(21) can be adjusted so that the two-component potential defined by these expressions satisfy the more restrictive boundary conditions mentioned above. To do this, we need an additional condition: the velocity field must satisfy certain equations of state as well. In brief, this requirement can be substantiated as follows.

Consider a sufficiently smooth vector field $\vec{u}$ satisfying the incompressibility condition (8), the impermeability condition with perfect slip, and the momentum equation (7) with admissible and sufficiently smooth $\rho = \rho(t,x)$, $\mu = \mu(t,x)$, and $p = p(t,x)$. Using the boundary conditions, we can represent the velocity field $\vec{u}$ as Fourier series:

$$u_1(t,x_1,x_2,x_3) = \tag{22}$$
$$\sum_{i=0}^{\infty}\sum_{j=0}^{\infty}\sum_{k=0}^{\infty} u^1_{ijk}(t)\sin(\frac{\pi i x_1}{l_1})\cos(\frac{\pi j x_2}{l_2})\cos(\frac{\pi k x_3}{l_3}),$$

$$u_2(t,x_1,x_2,x_3) = \tag{23}$$
$$\sum_{i=0}^{\infty}\sum_{j=0}^{\infty}\sum_{k=0}^{\infty} u^2_{ijk}(t)\cos(\frac{\pi i x_1}{l_1})\sin(\frac{\pi j x_2}{l_2})\cos(\frac{\pi k x_3}{l_3}),$$

$$u_3(t,x_1,x_2,x_3) = \tag{24}$$
$$\sum_{i=0}^{\infty}\sum_{j=0}^{\infty}\sum_{k=0}^{\infty} u^3_{ijk}(t)\cos(\frac{\pi i x_1}{l_1})\cos(\frac{\pi j x_2}{l_2})\sin(\frac{\pi k x_3}{l_3}).$$

Henceforth, the variable t is treated as a parameter. The velocity $\vec{u}$ can always be represented as $\vec{u} = \text{rot}\ \vec{\psi}$, where the three-component potential $\vec{\psi} = (\psi_1, \psi_2, \psi_3)$ satisfies more restrictive boundary conditions. Using the boundary conditions, we represent the components of $\vec{\psi}$ as Fourier series:

$$\psi_1(t,x_1,x_2,x_3) = \sum_{i=0}^{\infty}\sum_{j=0}^{\infty}\sum_{k=0}^{\infty}\psi^1_{ijk}(t)\cos(\frac{\pi i x_1}{l_1})\sin(\frac{\pi j x_2}{l_2})\sin(\frac{\pi k x_3}{l_3}), \tag{25}$$

$$\psi_2(t,x_1,x_2,x_3) = \sum_{i=0}^{\infty}\sum_{j=0}^{\infty}\sum_{k=0}^{\infty}\psi^2_{ijk}(t)\sin(\frac{\pi i x_1}{l_1})\cos(\frac{\pi j x_2}{l_2})\sin(\frac{\pi k x_3}{l_3}), \tag{26}$$

$$\psi_3(t,x_1,x_2,x_3) = \sum_{i=0}^{\infty}\sum_{j=0}^{\infty}\sum_{k=0}^{\infty}\psi^3_{ijk}(t)\sin(\frac{\pi i x_1}{l_1})\sin(\frac{\pi j x_2}{l_2})\cos(\frac{\pi k x_3}{l_3}). \tag{27}$$

Here, the Fourier coefficients obey the following constraints:

$$u^1_{ijk}(t) = \psi^3_{ijk}(t)\frac{\pi j}{l_2} - \psi^2_{ijk}(t)\frac{\pi k}{l_3},$$

$$u^2_{ijk}(t) = \psi^1_{ijk}(t)\frac{\pi k}{l_3} - \psi^3_{ijk}(t)\frac{\pi i}{l_1},$$

$$u^3_{ijk}(t) = \psi^2_{ijk}(t)\frac{\pi i}{l_1} - \psi^1_{ijk}(t)\frac{\pi j}{l_2}.$$

Substituting this representation of the vector potential into the variational equation (17) and consecutively using the test vector functions $\vec{\omega} = (\omega_1, 0, 0)$, $\vec{\omega} = (0, \omega_2, 0)$, and $\vec{\omega} = (0, 0, \omega_3)$ with

$$\omega_1 = \cos(\frac{\pi i x_1}{l_1})\sin(\frac{\pi j x_2}{l_2})\sin(\frac{\pi k x_3}{l_3}),$$

$$\omega_2 = \sin(\frac{\pi i x_1}{l_1})\cos(\frac{\pi j x_2}{l_2})\sin(\frac{\pi k x_3}{l_3}),$$

$$\omega_3 = \sin(\frac{\pi i x_1}{l_1})\sin(\frac{\pi j x_2}{l_2})\cos(\frac{\pi k x_3}{l_3}),$$

we obtain a system of linear equations that can be compactly written as

$$\begin{pmatrix} A_{11} & A_{12} & A_{13} \\ A_{21} & A_{22} & A_{23} \\ A_{31} & A_{32} & A_{33} \end{pmatrix} \begin{pmatrix} \psi^{(1)} \\ \psi^{(2)} \\ \psi^{(3)} \end{pmatrix} = \begin{pmatrix} \rho^{(1)} \\ \rho^{(2)} \\ 0 \end{pmatrix}. \tag{28}$$

The entries of the infinite matrices A_{pq} are constructed from the numbers

$$a^{1lmn}_{1ijk} = (J^2-K^2)(M^2-N^2)\mu^{css}_{ijklmn} + 4JMKN\mu^{ccc}_{ijklmn} + ILKN\mu^{ssc}_{ijklmn} + ILJM\mu^{scs}_{ijklmn},$$

$$a^{2lmn}_{1ijk} = LM(K^2-I^2)\mu^{scs}_{ijklmn} - IJ(M^2-N^2)\mu^{css}_{ijklmn} - 2IMKN\mu^{ccc}_{ijklmn} - JLKN\mu^{ssc}_{ijklmn},$$

$$a^{3lmn}_{1ijk} = LN(J^2-I^2)\mu^{ssc}_{ijklmn} - IK(N^2-M^2)\mu^{css}_{ijklmn} - 2IJMN\mu^{ccc}_{ijklmn} - JLMK\mu^{scs}_{ijklmn},$$

$$a^{1lmn}_{2ijk} = IJ(N^2-L^2)\mu^{scs}_{ijklmn} + LM(K^2-J^2)\mu^{css}_{ijklmn} - 2LJKN\mu^{ccc}_{ijklmn} - IMKN\mu^{ssc}_{ijklmn},$$

$$a^{2lmn}_{2ijk} = (I^2-K^2)(L^2-N^2)\mu^{scs}_{ijklmn} + 4ILKN\mu^{ccc}_{ijklmn} + JMKN\mu^{ssc}_{ijklmn} + ILJM\mu^{css}_{ijklmn},$$

$$a^{3lmn}_{2ijk} = MN(I^2-J^2)\mu^{ssc}_{ijklmn} - JK(N^2-L^2)\mu^{scs}_{ijklmn} - 2ILJN\mu^{ccc}_{ijklmn} - ILMK\mu^{css}_{ijklmn},$$

$$a^{1lmn}_{3ijk} = IK(M^2-L^2)\mu^{ssc}_{ijklmn} - LN(K^2-J^2)\mu^{css}_{ijklmn} - 2LJMK\mu^{ccc}_{ijklmn} - IJMN\mu^{scs}_{ijklmn},$$

$$a^{2lmn}_{3ijk} = JK(L^2-M^2)\mu^{ssc}_{ijklmn} - MN(K^2-I^2)\mu^{scs}_{ijklmn} - 2ILKM\mu^{ccc}_{ijklmn} - ILJN\mu^{css}_{ijklmn},$$

$$a^{3lmn}_{3ijk} = (I^2-J^2)(L^2-M^2)\mu^{ssc}_{ijklmn} + 4ILJM\mu^{ccc}_{ijklmn} + JMKN\mu^{scs}_{ijklmn} + ILKN\mu^{css}_{ijklmn},$$

where the following parameters are used:

$$\mu^{ccc}_{ijklmn} = \int_\Omega \mu\cos(\frac{\pi i x_1}{l_1})\cos(\frac{\pi l x_1}{l_1})\cos(\frac{\pi j x_2}{l_2}) \times \cos(\frac{\pi m x_2}{l_2})\cos(\frac{\pi k x_3}{l_3})\cos(\frac{\pi n x_3}{l_3})dx,$$

$$\mu^{css}_{ijklmn} = \int_\Omega \mu\cos(\frac{\pi i x_1}{l_1})\cos(\frac{\pi l x_1}{l_1})\sin(\frac{\pi j x_2}{l_2}) \times \sin(\frac{\pi m x_2}{l_2})\sin(\frac{\pi k x_3}{l_3})\sin(\frac{\pi n x_3}{l_3})dx,$$

$$\mu^{ssc}_{ijklmn} = \int_\Omega \mu\sin(\frac{\pi i x_1}{l_1})\sin(\frac{\pi l x_1}{l_1})\sin(\frac{\pi j x_2}{l_2}) \times \sin(\frac{\pi m x_2}{l_2})\cos(\frac{\pi k x_3}{l_3})\cos(\frac{\pi n x_3}{l_3})dx,$$

$$\mu^{scs}_{ijklmn} = \int_\Omega \mu\sin(\frac{\pi i x_1}{l_1})\sin(\frac{\pi l x_1}{l_1})\cos(\frac{\pi j x_2}{l_2}) \times \cos(\frac{\pi m x_2}{l_2})\sin(\frac{\pi k x_3}{l_3})\sin(\frac{\pi n x_3}{l_3})dx,$$

$$I = \frac{\pi i}{l_1},\quad J = \frac{\pi j}{l_2},\quad K = \frac{\pi k}{l_3},$$

$$L = \frac{\pi l}{l_1},\quad M = \frac{\pi m}{l_2},\quad N = \frac{\pi n}{l_3}.$$

To formulate the rule for constructing A_{pq} from a^{qlmn}_{pijk}, we introduce a one-dimensional indexing system for the equations and unknowns, using any one-to-one mapping $f : N_0 \times N_0 \times N_0 \to N_0$ such that any triple index $(i,j,k) \in N_0 \times N_0 \times N_0$ is mapped to an index $f(i,j,k) \in N_0$, where $N_0 = \{0, 1, 2, ...\}$. The entries $(a^q_p)_{\alpha\beta}$ of a matrix A_{pq} are now defined as $(a^q_p)_{\alpha\beta} = a^{qlmn}_{pijk}$, where $(l,m,n) = f^{-1}(\alpha)$ and $(i,j,k) = f^{-1}(\beta)$.

The components of the vectors $\rho^{(1)}$, $\rho^{(2)}$, $\psi^{(1)}$, $\psi^{(2)}$, $\psi^{(3)}$ are defined as

$$\rho^{(1)}_{f(l,m,n)} = \frac{\pi m}{l_2} \cdot g \cdot \int_\Omega \rho(t,x)$$
$$\times \cos(\frac{\pi l x_1}{l_1}) \cos(\frac{\pi m x_2}{l_2}) \sin(\frac{\pi n x_3}{l_3}) dx,$$
$$\rho^{(2)}_{f(l,m,n)} = -\frac{\pi l}{l_1} \cdot g \cdot \int_\Omega \rho(t,x)$$
$$\times \cos(\frac{\pi l x_1}{l_1}) \cos(\frac{\pi m x_2}{l_2}) \sin(\frac{\pi n x_3}{l_3}) dx,$$
$$\psi^{(1)}_{f(i,j,k)} = \psi^1_{ijk}(t),\ \psi^{(2)}_{f(i,j,k)} = \psi^2_{ijk}(t),\ \psi^{(3)}_{f(i,j,k)} = \psi^3_{ijk}(t).$$

If we multiply by $\pi l/l_1$, $\pi m/l_2$, and $\pi n/l_3$, respectively, each entry in the rows indexed by $f(l,m,n)$ in the sets of rows (A_{11}, A_{12}, A_{13}), (A_{21}, A_{22}, A_{23}), and (A_{31}, A_{32}, A_{33}) in (28) and add up the results, then we obtain a zero row, because

$$\frac{\pi l}{l_1} \cdot a^{qlmn}_{1ijk} + \frac{\pi m}{l_2} \cdot a^{qlmn}_{2ijk} + \frac{\pi n}{l_3} \cdot a^{qlmn}_{3ijk} = 0,$$
$$q = 1,2,3, \quad i,j,k,l,m,n \in N_0.$$

As a result, we set to zero the last set of rows in the matrix of system (28). The elements in the column of absolute terms remain zero as well, because

$$\frac{\pi l}{l_1} \cdot \rho^{(1)}_{f(l,m,n)} + \frac{\pi m}{l_2} \cdot \rho^{(2)}_{f(l,m,n)} + \frac{\pi n}{l_3} \cdot 0 = 0, \quad l,m,n \in N_0.$$

This means that the vectors $\psi^{(1)}$, $\psi^{(2)}$, and $\psi^{(3)}$ satisfy the system of linear equations

$$\begin{pmatrix} A_{11} & A_{12} & A_{13} \\ A_{21} & A_{22} & A_{23} \\ 0 & 0 & 0 \end{pmatrix} \begin{pmatrix} \psi^{(1)} \\ \psi^{(2)} \\ \psi^{(3)} \end{pmatrix} = \begin{pmatrix} \rho^{(1)} \\ \rho^{(2)} \\ 0 \end{pmatrix}. \tag{29}$$

Moreover, the linear dependence of rows in the matrix of system (28) implies that systems (28) and (29) are equivalent. These systems are solvable since $\vec{\psi}$ satisfies the variational equation. The columns of the matrices of systems (28) and (29) are also linearly dependent, because

$$\frac{\pi i}{l_1} \cdot a^{1lmn}_{pijk} + \frac{\pi j}{l_2} \cdot a^{2lmn}_{pijk} + \frac{\pi k}{l_3} \cdot a^{3lmn}_{pijk} = 0,$$
$$p = 1,2,3, \quad i,j,k,l,m,n \in N_0.$$

Therefore, the solvability of (29) entails the solvability of the system

$$\begin{pmatrix} A_{11} & A_{12} \\ A_{21} & A_{22} \end{pmatrix} \begin{pmatrix} \psi^{(1)}_* \\ \psi^{(2)}_* \end{pmatrix} = \begin{pmatrix} \rho^{(1)} \\ \rho^{(2)} \end{pmatrix}, \tag{30}$$

and its solution is given by the vectors $\psi^{(1)}_*$ and $\psi^{(2)}_*$ whose components are

$$\psi^{(1)}_{*f(i,j,k)} = \psi^{(1)}_{f(i,j,k)} - \frac{il_3}{kl_1} \cdot \psi^{(3)}_{f(i,j,k)},$$
$$\psi^{(2)}_{*f(i,j,k)} = \psi^{(2)}_{f(i,j,k)} - \frac{jl_3}{kl_2} \cdot \psi^{(3)}_{f(i,j,k)},$$
$$i,j,k \in N_0, \quad k \neq 0,$$
$$\psi^{(1)}_{*f(i,j,0)} = 0, \quad \psi^{(2)}_{*f(i,j,0)} = 0, \quad i,j \in N_0.$$

The reverse proposition is also valid: if vectors $\psi^{(1)}_*$ and $\psi^{(2)}_*$ constitute a solution to system (30), then the vectors $\psi^{(1)} = \psi^{(1)}_*$, $\psi^{(2)} = \psi^{(2)}_*$, and $\psi^{(3)} = 0$ constitute a solution to both (29) and (28).

The analysis above implies that one may set $\psi^{(3)} = 0$ when considering systems (29) and (28). Therefore, the velocity field $\vec{u}$ can be represented as in (18), where the potential $\vec{\psi} = (\psi_1, \psi_2, 0)$ satisfies the more restrictive boundary conditions corresponding to impermeability with perfect slip.

Now, we consider the case of no-slip conditions. The corresponding representation (18) subject to more restrictive no-slip conditions is relatively simple to find when viscosity has the form $\mu = \mu(t, x_3)$ or $\mu = \mu(t, x_1, x_2)$. This assertion can be validated by an analysis that does not rely on the scheme developed above for the impermeability conditions with perfect slip. However, the desired representation (18) has been neither proved nor disproved in the case when viscosity has the general form $\mu = \mu(t, x)$.

Remark. The problem formulated for a horizontally uniform viscosity $\mu = \mu(t, x_3)$ can be substantially simplified by replacing a three-component potential $\vec{\psi} = (\psi_1, \psi_2, \psi_3)$ or a two-component potential $\vec{\psi} = (\psi_1, \psi_2, 0)$ with the single-component potential

$$\vec{\psi} = \mathrm{curl}(\varphi \vec{e}_3) = (\partial\varphi/\partial x_2, -\partial\varphi/\partial x_1, 0), \tag{31}$$

where $\varphi = \varphi(t, x)$ is a scalar function satisfying appropriate boundary conditions. This can be done because the velocity field $\vec{u}$ can be represented as $\vec{u} = \mathrm{rot\ rot}\ (\varphi \vec{e}_3)$ (note that this representation is not unique). Omitting a detailed analysis, we can define the scalar function φ as a solution to the equation

$$\frac{\partial^2 \varphi}{\partial x_1^2} + \frac{\partial^2 \varphi}{\partial x_2^2} = -u_3 \ \ in\ \ \overline{\Omega}.$$

In the case of impermeability conditions with perfect slip, this solution must satisfy the boundary conditions

$$\Gamma(x_1 = 0, x_1 = l_1) : \partial\varphi/\partial x_1 = 0;$$
$$\Gamma(x_2 = 0, x_2 = l_2) : \partial\varphi/\partial x_2 = 0;$$
$$\Gamma(x_3 = 0, x_3 = l_3) : \varphi = 0 = \partial^2\varphi/\partial x_3^2;$$

in the case of no-slip conditions, it should satisfy the boundary conditions

$$\Gamma(x_1 = 0, x_1 = l_1) : \varphi = 0 = \partial\varphi/\partial x_1;$$
$$\Gamma(x_2 = 0, x_2 = l_2) : \varphi = 0 = \partial\varphi/\partial x_2;$$
$$\Gamma(x_3 = 0, x_3 = l_3) : \varphi = 0 = \partial\varphi/\partial x_3.$$

Thus, the determination of $\vec{u}$ for $\mu = \mu(t, x_3)$ can be

reduced to computing a single scalar function φ that satisfies both the corresponding simplified version of Eqs. (13)–(15) (or simplified variational equation (17)) and appropriate boundary conditions. In this case, it should be kept in mind that

$$u_1 = -\partial^2\varphi/\partial x_1\partial x_3, \quad u_2 = \partial^2\varphi/\partial x_2\partial x_3,$$

$$u_3 = -\partial^2\varphi/\partial x_1^2 - \partial^2\varphi/\partial x_2^2.$$

7 APPROXIMATION OF THE PROBLEM

Now we consider some universal aspects of approximate solution to the basic equations for the desired functions. For example, the vector potential $\vec{\psi}$ can be found, together with the thermally unperturbed density ρ_* and viscosity μ_*, by applying a finite element method with basis functions of a special form. The construction of the basis functions and the implementation of the finite element method were described in detail by Ismail-Zadeh et al. (1998). Here, the vector potential is also approximated by a linear combination of tricubic basis functions expressed as tensor products of appropriate cubic splines:

$$\psi_p(t,x_1,x_2,x_3) \approx \sum_{i=0}^{n_1}\sum_{j=0}^{n_2}\sum_{k=0}^{n_3}\psi_{ijk}^{(p)}(t)s_i^{(p1)}(x_1)s_j^{(p2)}(x_2)s_k^{(p3)}(x_3), \quad p=1,2. \tag{32}$$

Density and viscosity are approximated by linear combinations of appropriate trilinear basis functions expressed as tensor products of linear functions:

$$\rho_*(t,x_1,x_2,x_3) \approx \sum_{i=0}^{n_1}\sum_{j=0}^{n_2}\sum_{k=0}^{n_3}\rho_{ijk}(t)\tilde{s}_i^{(1)}(x_1)\tilde{s}_j^{(2)}(x_2)\tilde{s}_k^{(3)}(x_3), \tag{33}$$

$$\mu_*(t,x_1,x_2,x_3) \approx \sum_{i=0}^{n_1}\sum_{j=0}^{n_2}\sum_{k=0}^{n_3}\mu_{ijk}(t)\tilde{s}_i^{(1)}(x_1)\tilde{s}_j^{(2)}(x_2)\tilde{s}_k^{(3)}(x_3). \tag{34}$$

Trilinear basis functions provide good approximations of discontinuous fluid properties.

By substituting approximations (32)–(34) into (17), the approximate vector potential is found for prescribed density and viscosity distributions by solving a system of linear algebraic equations with a positive definite band matrix for the unknown coefficients $\{\psi_{ijk}^{(p)}(t)\}$. However, the condition number of the system tends to infinity as the grid is condensed. This leads to difficulties in solving high-dimensional systems, since iterative methods tend to exhibit progressively slow convergence, and may even diverge in some cases because of roundoff errors. Here, a solution is obtained by directly applying the square-root method. Some versions of this method implemented on parallel computers were described by Ortega (1991), Ismail-Zadeh et al. (1998), Korotkii et al. (1999), and Ismail-Zadeh et al. (2000).

Substituting approximations (33) and (34) into (12), we computed approximations of the thermally unperturbed density and viscosity for a prescribed velocity distribution by the method of characteristics, i.e., by transferring the initial conditions along the characteristics of Eqs. (12) (for details, see Ismail-Zadeh et al. 1998). This method can be used in computations with relatively weak density and viscosity dissipations (Marchuk 1989; Ismail-Zadeh et al. 1998; Korotkii et al. 1999). The characteristics of transport equations are defined by systems of ordinary differential equations of the form (e.g., see Ladyzhenskaya 1970; Antontsev et al. 1983; Marchuk 1989)

$$dx(t)/dt = \vec{u}(t,x(t)).$$

The thermally unperturbed density and viscosity have constant values on the characteristics:

$$\rho_*(t,x(t)) = \rho_0(x(t_0)), \quad \mu_*(t,x(t)) = \mu_0(x(t_0)), \quad t \geq t_0.$$

These relations can be used to find density and viscosity in Ω at $t > t_0$ for the prescribed initial density and viscosity distributions, provided that the velocity fields at t have already been computed. When trilinear basis functions are used to approximate density and viscosity, a sufficiently large number of independent modules can be organized to compute the characteristics of transport equations and the corresponding densities and viscosities on them. Note that a finer grid can be used to approximate both density and viscosity, as compared to the grid used for computing the vector potential.

The temperature $T = T(t,x)$ was approximated by finite-difference methods. The derivatives $\partial u_i/\partial x_j$ were determined by differentiating the relation $\vec{u} = \text{rot}\ \vec{\psi}$ with the use of (32). Temperature was computed by the implicit alternating-direction method (Marchuk 1989). At each iteration step in time, a large set of linear algebraic systems with tridiagonal matrices was solved, and a corresponding number of independent modules could be organized for parallel solution of these systems by means of tridiagonal algorithms.

In summary, the numerical solution of the problem consisted of the following basic stages: (1) a set of linear algebraic equations was solved for the coefficients of a decomposition of the vector velocity potential in terms of basis functions, (2) the heat equation was integrated, and (3) the equations for advection of density and viscosity were inte-

grated. All of these stages require substantial computing resources.

8 COMPUTATIONAL PROCEDURE

Here we describe briefly the procedure of solving the problem. A uniform discretization of the time axis, $t_n = t_0 + \tau n$ ($n \in Z$), is defined a priori, where τ is the discretization parameter. Next, an iterative process is organized in which n is consecutively assigned integer values ranging from 0 to m. (The integer m is prescribed prior to computations to set the length of the interval $[t_0, t_m]$ of integration). When necessary, the process can be continued further, starting from t_m as an initial time. At each iteration step in time, the following three steps are executed sequentially.

Step 1. The distributions of temperature, $T = T(t_n, \cdot)$, and thermally unperturbed density and viscosity, $\rho_* = \rho_*(t_n, \cdot)$ and $\mu_* = \mu_*(t_n, \cdot)$, at $t = t_n$ are used to determine from (10) and (11) the thermally perturbed $\rho = \rho(t_n, \cdot)$ and $\mu = \mu(t_n, \cdot)$ at the same $t = t_n$. Then, the distribution of $\vec{\psi} = \vec{\psi}(t_n, \cdot)$ is found by solving Eqs. (13)–(15) or variational equation (17), and (8) is used to calculate the velocity $\vec{u} = \vec{u}(t_n, \cdot)$.

Step 2. The distributions of velocity, $\vec{u} = \vec{u}(t_n, \cdot)$, and thermally perturbed density and viscosity, $\rho = \rho(t_n, \cdot)$ and $\mu = \mu(t_n, \cdot)$, are used to compute a new temperature distribution $T = T(t_{n+1}, \cdot)$ at $t = t_{n+1}$ by solving Eq. (9) supplemented by boundary conditions.

Step 3. The distributions of velocity, $\vec{u} = \vec{u}(t_n, \cdot)$, and thermally unperturbed density and viscosity, $\rho_* = \rho_*(t_n, \cdot)$ and $\mu_* = \mu_*(t_n, \cdot)$, are used to compute new thermally unperturbed density and viscosity, $\rho_* = \rho_*(t_{n+1}, \cdot)$ and $\mu_* = \mu_*(t_{n+1}, \cdot)$, at $t = t_{n+1}$ by solving Eq. (12).

The iterative process results in distributions of temperature $T = T(t_n, \cdot)$, potential vector $\vec{\psi} = \vec{\psi}(t_n, \cdot)$, velocity $\vec{u} = \vec{u}(t_n, \cdot)$, and thermally unperturbed density $\rho_* = \rho_*(t_n, \cdot)$ and viscosity $\mu_* = \mu_*(t_n, \cdot)$ as well as thermally perturbed density $\rho = \rho(t_n, \cdot)$ and viscosity $\mu = \mu(t_n, \cdot)$, at $t = t_n$ ($n = 0, ..., m$). Once these distributions are available, the evolution of the system on the interval $[t_0, t_m]$ can be recovered in more detail by interpolation. The time step can be chosen automatically so that the largest displacement of fluid elements does not exceed a preset small amount.

9 NUMERICAL EXAMPLE

As a typical example, we computed a flow in the parallelepiped $\Omega = [0, 3] \times [0, 3] \times [0, 1]$. At $t_0 = 0$, we set $\rho_*^0(x) \equiv 1$, $\mu_*^0(x) \equiv 1$, and $T_*^0(x) = 1.05 - x_3/l_3$. On the faces $\Gamma(x_3 = l_3)$ and $\Gamma(x_3 = 0)$, we set $T_2 \equiv 0.05$ and $T_1 \equiv 1.05$, respectively. We set $Q = 0$ and restricted ourselves to the case of impermeability conditions with perfect slip. The values of physical parameters given in Section 2 were adopted in the modeling. We introduced a small temperature disturbance at $x_0 = (3/2, 3/2, 1/3)$ at the initial time, which led to the development of a thermal diapir (or plume).

We used a $25 \times 25 \times 25$ grid for vector potential and viscosity and a $73 \times 73 \times 73$ grid for density and temperature. The time step was set equal to 0.1. Table 1 shows the processing characteristics of various parallel computers with distributed memory used to compute our numerical example.

Figure 1 illustrates the shapes of isotherm $T = 0.9$ computed at successive times. The numerical results are consistent with those obtained in analyzing the Rayleigh-Benard instability at small overcritical Rayleigh numbers (Chandrasekhar 1968) and two-dimensional thermal convection (Trompert & Hansen 1998).

10 CONCLUSIONS

We proposed a numerical approach to the problem of slow, highly viscous, incompressible flows with temperature-dependent density and viscosity under gravitational and thermal effects. The approach relies on a finite element method and a representation of a two-component vector velocity potential for an incompressible viscous fluid by a linear combination of tricubic splines with unknown coefficients. The use of tricubic splines leads to a highly accurate solution to the problem, as compared to other finite-different or finite-element methods, while the discrete approximations employed have relatively low dimensions. The advection equations for density and viscosity are solved by the method of characteristics; the heat balance equation, by means of a tridiagonal algorithm.

The two-component representation (18) of the vector potential proposed in this study is computationally advantageous as compared to the two-component representation

$$\vec{u} = \mathrm{curl}\vec{\psi}, \quad \vec{\psi} = \mathrm{curl}(\varphi_1 \vec{e}_3) + \varphi_2 \vec{e}_3, \tag{35}$$

with scalar poloidal and toroidal potentials φ_1 and φ_2 (e.g., see Chandrasekhar 1968; Busse & Frick 1985; Christensen & Harder 1991). Representation (18) is simpler than (35). It entails simple relations (19)–(21) between the components of the velocity and potential vectors, which are equivalent to $u_1 = -\partial\psi_2/\partial x_3$, $u_2 = \partial\psi_1/\partial x_3$, and $u_3 = \partial\psi_2/\partial x_1 - \partial\psi_1/\partial x_2$. When representation (35) is used, one has to deal with equations of higher order as compared to Eqs. (13)–(15), which require a more cumbersome and complicated

Table 1. Operational characteristics of various parallel computers.

Computer	No. of processors	Time	CPU	Communication rate
MVS–100	30	180'	I860/80 MHz	1 Mb/s
MVS–1000	8	7'15"	Alpha/300 MHz	10 Mb/s
Alpha	2	55'	Alpha/540 MHz	10 Mb/s
IBM SP2	16	3'25"	RS6000/133 MHz	3 Mb/s

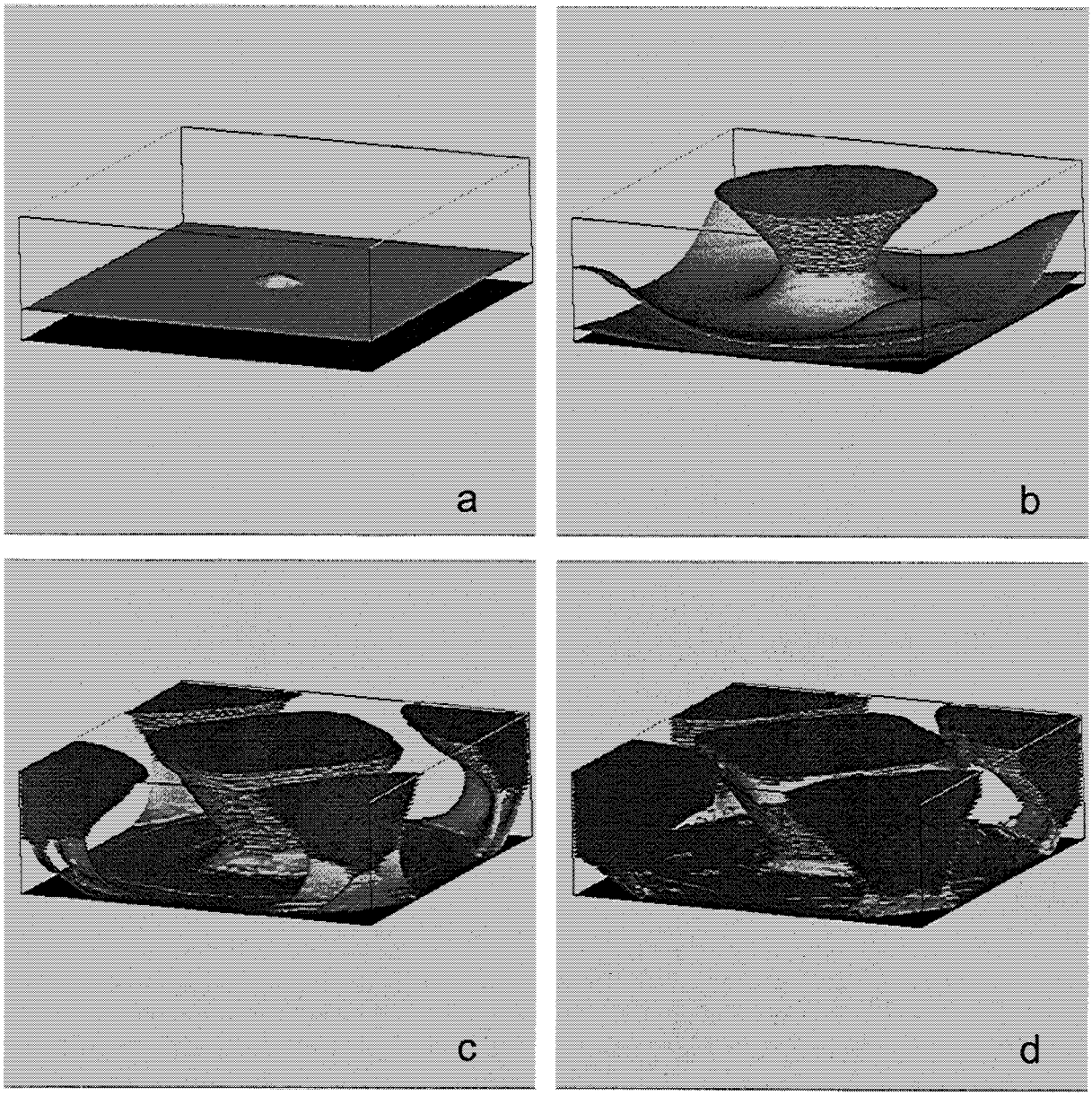

Figure 1. Evolution of thermal plume at time t: 0 *(a)*, 120 *(b)*, 150 *(c)*, and 180 *(d)*.

numerical analysis. Moreover, representation (18) is valid not only in the domain Ω. It remains valid under the additional requirement that the boundary conditions considered here are consistently satisfied by the velocity vector and the corresponding vector potential. It is also important that the contributions previously made by various authors, including those published in (Ismail-Zadeh et al. 1998, 2000; Korotkii

et al. 1999), as well as available software, remain effective and may even turn out to be more efficient.

A greater part of computational resources is required to solve the system of linear algebraic equations obtained by discretizing the variational equation (17). The corresponding algorithm factorizes the matrix of the linear system and solves the resulting linear systems with upper and lower triangular matrices. The square root method (Choleskii method) is advantageous in that the solution is obtained up to the computer arithmetic accuracy. Its disadvantages include higher requirements for memory and CPU time resources. Iterative (e.g., Gauss–Seidel or Schwarz) methods require much less memory, but test computations have shown that the convergence rates of the iterative processes are too low. The multigrid iterative approach is also disadvantageous as applied to simulate thermally driven convection, since the corresponding convergence rate is too low when large variations of viscosity are to be computed (Tackley 1993; Trompert & Hansen 1996). When the conjugate gradient method is applied, convergence cannot be improved to an acceptable degree, whereas the CPU time increases immensely (Trompert & Hansen 1998). It should be kept in mind that a high numerical accuracy is essential for computing the evolution of unstable flows, which are extremely sensitive to small disturbances (such as those resulting from numerical errors). This motivates the use of the highly accurate square root method for solving such problems. When the two-component velocity potential and, in some cases, the one-component potential proposed here are employed, the computing resources and CPU times required to solve the systems of equations are substantially reduced, and the basic disadvantage of the present approach is thereby eliminated.

The principal results of this study are summarized as follows:

1. We develop a numerical method for simultaneous solution of the Stokes flow equation, heat balance equation, and advection equations for physical parameters of the fluid.

2. We show that computational costs can be reduced by an introduction of two-component (or even one-component in some cases) representation of vector potential.

3. Numerical test experiments are carried out for a three-dimensional model of thermal convection.

ACKNOWLEDGMENTS

This research was supported by the International Science and Technology Center (project No. 1293-99) and by the Russian Foundation for Basic Research (project Nos. 99-05-65050 and 99-07-90441).

REFERENCES

Antontsev, S.N., Kazhikhov, A.V. & Manakhov, V.N. *Boundary-value Problems in Mechanics of Heterogeneous Fluids*, Novosibirsk, Nauka, 1983 (in Russian).

Busse, F.H. & Frick H., Square pattern convection in fluids with strongly temperature-dependent viscosity, *J. Fluid Mech., 150,* 451–465, 1985.

Chandrasekhar, S. *Hydrodynamic and Hydromagnetic Stability*, Oxford, Clarendon Press, 1968.

Christensen, U. & Harder, H., 3-D convection with variable viscosity, *Geophys. J. Int., 104,* 213–226, 1991.

Cserepes, L., Rabinowicz, M. & Rosemberg-Borot, C., Three-dimensional convection in a two-layer mantle, *J. Geophys. Res., 93*, 12009–12025, 1988.

Frick, H., Busse, F.H. & Clever, R.M., Steady three-dimensional convection at high Prandtl number, *J. Fluid Mech., 127*, 141–153, 1983.

Houseman, G., The dependence of convection planform on mode of heating, *Nature, 332,*, 346–349, 1988.

Ismail-Zadeh, A.T., B.M. Naimark & Lobkovsky, L.I., Hydrodynamic model of sedimentary basin formation based on development and subsequent phase transformation of a magmatic lens in the upper mantle, *Comput. Seis. Geodyn., 3*, 42-53, 1996.

Ismail-Zadeh, A.T., Korotkii, A.I., Naimark, B.M., Suetov, A.P. & Tsepelev, I.A., Implementation of a three-dimensional hydrodynamic model for evolution of sedimentary basins, *Comput. Math. & Mathl Phys., 38,* 1138–1151, 1998.

Ismail-Zadeh, A.T., Tsepelev, I.A., Talbot, C. & Oster, P., A numerical method and parallel algorithm for three-dimensional modeling of salt diapirism, in *Problems in Dynamics and Seismicity of the Earth* (Eds. V.I. Keilis-Borok and G.M. Molchan), pp.62–76, GEOS, Moscow, 2000 (in Russian).

Korotkii, A.I., Tsepelev, I.A., Ismail-Zadeh, A.T. & Naimark, B.M., Parallel algorithms for modelling of inhomogeneous viscous flow, *Proc. Ural State Univ., 14,* 65–76, 1999 (in Russian).

Ladyzhenskaya, O.A., *Mathematical Problems of Dynamics of Viscous Incompressible Fluid*, Moscow, Nauka, 1970 (in Russian).

Landau, L.D. & Lifshitz, E.M., *Fluid Mechanics*, Oxford, Pergamon Press, 1987.

Marchuk, G.I., *Methods of Computational Mathematics*, Moscow, Nauka, 1989 (in Russian).

McKenzie, D.P., Roberts, J.M. & Weiss, N.O., Convection in the Earth's mantle: towards a numerical simulation, *J. Fluid Mech., 62*, 465–538, 1974.

Naimark, B.M., Existence and uniqueness of the solution of the Rayleigh-Taylor problem, *Comput. Seis., 18,* Allerton Press, 32–41, 1987.

Naimark, B.M., Existence and uniqueness in the small of the solution of the Rayleigh-Benard problem, *Comput. Seis., 21,* Allerton Press, 87–105, 1989.

Ogawa, M., Schubert, G. & Zebib, A., Numerical simulation of

three-dimensional thermal convection in a fluid with strongly temperature-dependent viscosity, *J. Fluid Mech., 233,* 299–328, 1991.

Ortega, J.M., *Introduction to Parallel and Vector Solution of Linear Systems*, Plenum Press, New York, 1988.

Rykov, V.V. & Trubitsyn, V.P., 3D model of mantle convection incorporating moving continents, *Comput. Seis. Geodyn., 3*, 42-53, 1996.

Tackley, P.J., Effects of strongly temperature-dependent viscosity on time-dependent, three-dimensional models of mantle convection, *Geophys. Res. Lett., 20*, 2187–2190, 1993.

Travis, B., Olson, P. & Schubert, G., The transition from two-dimensional to three-dimensional planforms in infinite-Prandtl-number thermal convection, *J. Fluid Mech., 216,* 71–91, 1990.

Turcotte, D.L. & Schubert, G. *Geodynamics: Application of Continuum Physics to Geological Problems*, John Willey & Sons, New York, 1982.

Trompert, R.A. & Hansen, U., The application of a finite volume multigrid method to three-dimensional flow problems in a highly viscous fluid with a variable viscosity, *Geophys. Astrophys. Fluid Dynamics., 83*, 261–291, 1996.

Trompert, R.A. & Hansen, U., On the Rayleigh number dependence of convection with a strongly temperature-dependent viscosity, *Phys. Fluid., 10(2)*, 351–360, 1998.